

1 **Untangling intercropping in heterogeneous smallholder maize-cassava farming systems**  
2 **with remote sensing**  
3

4 Felicia O. Akinyemi<sup>a,b,1\*</sup>, Philippe Rufin<sup>c,d</sup>, Esther Shupel Ibrahim<sup>d,e,f</sup>, Patrick Hostert<sup>d,g</sup>,  
5 Lucia O. Ogunsumi<sup>h</sup>, Olugbenga A. Egbetokun<sup>h</sup>, Chinwe Ifejika Speranza<sup>a</sup>

6 <sup>a</sup>Land Systems and Sustainable Land Management, Institute of Geography, University of Bern,  
7 Hallerstrasse 12, 3012 Bern, Switzerland; felicia.akinyemi@unibe.ch;  
8 chinwe.ifejika.speranza@unibe.ch

9 <sup>b</sup>Geomatics, Department of Environmental and Life Sciences, Karlstads University, Universitetsgatan  
10 2, 651 88 Karlstad, Sweden; felicia.akinyemi@kau.se

11 <sup>c</sup>Earth and Life Institute, UCLouvain, Place Louis Pasteur 3, 1348 Louvain-La-Neuve, Belgium;  
12 philippe.rufin@uclouvain.be

13 <sup>d</sup>Geography Department, Humboldt-Universität zu Berlin, Unter den Linden 6, 10099 Berlin, Germany;  
14 esther.shupel.ibrahim@hu-berlin.de; patrick.hostert@geo.hu-berlin.de

15 <sup>e</sup>Leibniz Centre for Agricultural Landscape Research, Eberswalder Straße 84, 15374 Müncheberg,  
16 Germany

17 <sup>f</sup>National Centre for Remote Sensing, Jos, Rizek Village Jos Eat LGA, P.M.B. 2136 Jos, Plateau State,  
18 Nigeria

19 <sup>g</sup>IRI THESys – Integrative Research Institute on Transformations of Human-Environment Systems,  
20 Humboldt-Universität zu Berlin, Unter den Linden 6, 10099 Berlin, Germany

21 <sup>h</sup>Institute of Agricultural Research and Training, Obafemi Awolowo University, Moor Plantation,  
22 Ibadan, Nigeria; lucyogunsumi2011@gmail.com; oaegbetokun@gmail.com

23  
24  
25 *This paper is a non-peer reviewed preprint submitted to EarthArXiv. It has been submitted to the Remote*  
26 *Sensing of Environment for peer review.*  
27

---

<sup>1</sup> \*Corresponding author. Land Systems and Sustainable Land Management, Institute of Geography, University of Bern, Hallerstrasse 12, 3012 Bern, Switzerland, akinyemi.felicia@gmail.com +41 779693968.

29 Earth observation approaches for large-scale crop monocultures are often not transferable to  
30 heterogeneous smallholder systems. Key challenges in this regard are intercropping, high intra-  
31 field crop type variability, wide sowing windows, presence of non-crop vegetation and small  
32 but variable field sizes. Currently, studies on smallholder agriculture mainly focus on specific  
33 crops and seldom account for crop mixtures or multiple growing cycles. Moreover, our  
34 knowledge about ongoing processes of farm consolidation and effects on intercropping remains  
35 limited due to the absence of spatially detailed information on field size. We mapped  
36 monocropping and maize-cassava intercropping in 2022/2023 and the relationship with field  
37 sizes. We combined Sentinel-1 radar and optical Sentinel-2 time series to classify farming  
38 systems across two growing cycles in the Guinea Savannah of southwest Nigeria. We tested  
39 spectral-temporal features at monthly and bimonthly intervals for the growing season and off-  
40 season. We used deep transfer learning to fine-tune a pre-trained convolutional neural network  
41 designed for crop field delineation. Using very high resolution imagery (0.6 m) for a regularly  
42 distributed sample across the study region (n=2,333), mean overall accuracy based on k-fold  
43 cross-validation was 0.79 (+/-0.02%), whereas User and Producer accuracies were above 0.70  
44 for most classes. Sentinel-1 alone underperformed, while models using only Sentinel-2 had  
45 higher overall accuracies but suffered from cloud-induced data gaps. Field size estimation  
46 revealed a high spatial agreement with mean intersection over union scores of up to 0.73 in site-  
47 level field size estimation. Small and medium-sized fields were dominant. Monocropping was  
48 positively related to field sizes as larger monocropping fields of early-planted cassava, late-  
49 planted maize, yam and rice clustered in the North of our study region. In contrast, smaller  
50 intercropped fields of maize-cassava mainly occurred in fragmented agricultural landscapes  
51 with ample natural vegetation. Our approach demonstrates the potential of integrating radar and  
52 optical time series in cloud-prone regions for mapping crop mixtures in complex forest-  
53 agricultural mosaic landscapes during multiple growing cycles. Our study provides a valuable  
54 workflow for producing timely information for the quantification of crop production in  
55 heterogeneous smallholder farming systems.

56

57

58

59

60

61

62

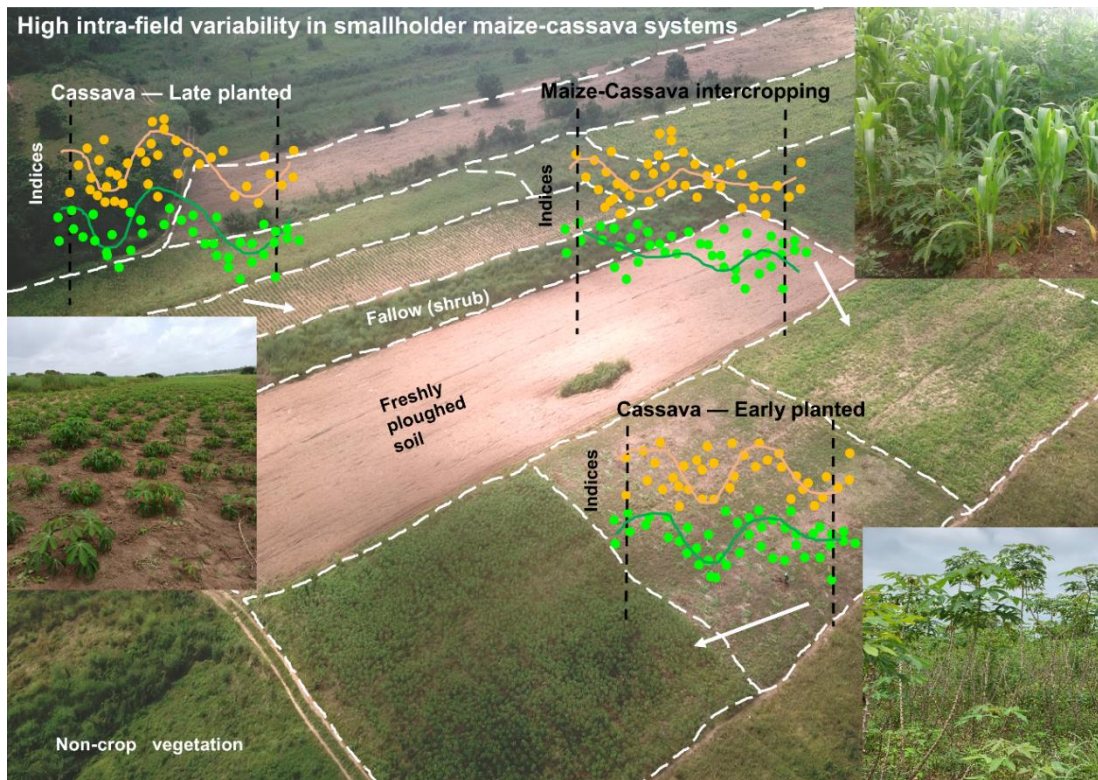
63

64

65

66 Graphical abstract

67



68

69

70 Keyword

71 Spectral-temporal features, smallholder, mixed farming, Sentinel 1 - 2, Random Forest,  
72 Automated field delineation

73 Highlights

74 ● Mapped intercropping in mixed crop farming and double growing cycles in smallholder  
75 farming systems

76 ● Best model for predicting crop types combined Sentinel-1 at monthly and Sentinel-2 at  
77 bimonthly intervals

78 ● Mapping early and late planted crops better reflects the local agroclimatic context

79  
80 ● Detailed field size delineation and estimates were efficiently obtained with deep transfer  
81 learning

82 ● Monocropping was positively related to field size in the Nigerian lower Guinea  
83 Savannah

# 1. Introduction

Remote Sensing provides timely and cost-efficient input for agricultural monitoring across large regions for pre- and within-growing season decision support (Johnson, 2014). Most approaches currently applied for mapping crop types were developed for large-scale crop monocultures, especially in industrialized economies (Fritz et al., 2019; Taiwo et al., 2023; Becker-Reshef et al., 2023). However, these approaches have limited applicability in heterogeneous agricultural systems such as those dominating smallholder agriculture worldwide, especially in developing countries. Smallholder farms are often heterogeneous and small, loosely defined by farm sizes of < 2 - 5 ha (FAO, 2014; Samberg et al., 2016; Fatunbi et al., 2020; Lowder et al., 2021). As smallholder agriculture produces about 30-34% of the global food supply, it is vital to reaching the Sustainable Development Goal (SDG) 2, which is concerned with ending hunger, achieving food security, improving nutrition and promoting sustainable agriculture (United Nations, 2015; FAO, 2016; Ricciardi et al., 2018).

Mapping crop types and their associated cropping patterns (i.e., mono- and mixed cropping) in smallholder contexts from remote sensing is challenging, especially for intercropping, a type of mixed farming characterized mainly by the simultaneous presence of multiple crops (Akinyemi, 2017; Kinyua et al., 2023). Intercropping is a traditional method of agricultural intensification aimed at increasing food production per unit of land and minimizing the risks of crop failure due to impacts such as drought and pests (Olasantan et al., 1996; Ayoola and Makinde, 2007; Bouws and Finckh, 2008; Nwokoro et al., 2021). Aside from the tendency for smallholder farms to be heterogeneous and small, notable constraining factors are the high intra-field variability in crop types and non-crop vegetation, the wide sowing windows and the lack of reference data for the mixed farming systems (Ibrahim et al., 2021). As elsewhere in the tropics, the lack of cloud-free optical images to map smallholder agriculture during much of the growing season necessitates combining images from different sensors, which is helpful for crop

110 type mapping in some smallholder contexts (e.g., Kpienbaareh et al., 2019; Rao et al., 2021;  
111 Ren et al., 2022). These factors compound the difficulty of mapping crop types and  
112 intercropping, especially distinguishing the phenology of multiple crops at different growth  
113 stages. Consequently, regional-scale crop type mapping approaches in intercropping systems  
114 have mainly focused on specific crops and often do not consider crop mixtures or multiple  
115 growing cycles.

116 This study considers the Lower Guinea Savannah (LGS), a predominantly smallholder  
117 agricultural region in the southwest of Nigeria. Historically, agricultural programmes  
118 implemented in this region have aimed at harnessing more arable lands for agriculture, hence  
119 the link to cropland expansion (Ekong, 1983; Akinyemi and Ifejika Speranza, 2022). Examples  
120 of such programmes are the farm settlement scheme of the 1950s, providing incentives for land  
121 and farm input (Ministry of Agriculture and Natural Resources, 1959) and the trade  
122 liberalization policy of the 1980s and 1990s prioritizing smallholder export-oriented cash crop  
123 production (Akinyemi, 2013). With the co-existence of various farming systems, the LGS  
124 presents a good case to predict crop types and map intercropping during multiple growing  
125 cycles in smallholder regions.

126 Despite intercropping being the dominant agricultural practice among smallholder  
127 farmers in Nigeria, as elsewhere in Africa where small- and large scale commercial  
128 monocropping systems using mechanization are emerging (Muyanga et al., 2019; Omotilewa  
129 field size is increasing (Ibrahim et al., 2021; Chiaka et al., 2022). Using the classes in the global  
130 study of field size distribution (Lesiv et al., 2019), Nigeria has 56% of very small fields (<0.64  
131 ha), 31% small fields (0.64 - 2.56 ha), 11% medium fields (2.56 - 16 ha), 2% large fields (16 -  
132 100 ha) and 1% very large fields (>100 ha). However, spatially explicit information on field  
133 size and the relationship to cropping patterns remains largely unknown. Therefore, we tested  
134 the detection of individual smallholder fields at very high spatial resolution utilizing deep

135 transfer learning and relating field size to cropping systems. We hypothesized that field size is  
136 related to the cropping system, with larger fields more likely being monocropped and smaller  
137 fields instead being cultivated in a mixed farming regime. This study's objectives were as  
138 follows:

- 139 • Develop a framework most suitable for predicting and mapping multiple crops and  
140 intercropping by combining spectral-temporal features of S1 and S2
- 141 • Map multiple crops and differentiate the cropping patterns (i.e., mono- and  
142 intercropping), considering there are two growing cycles per year
- 143 • Assess how field size relates to cropping patterns in smallholder farming systems

144

## 145 **2. Data and methods**

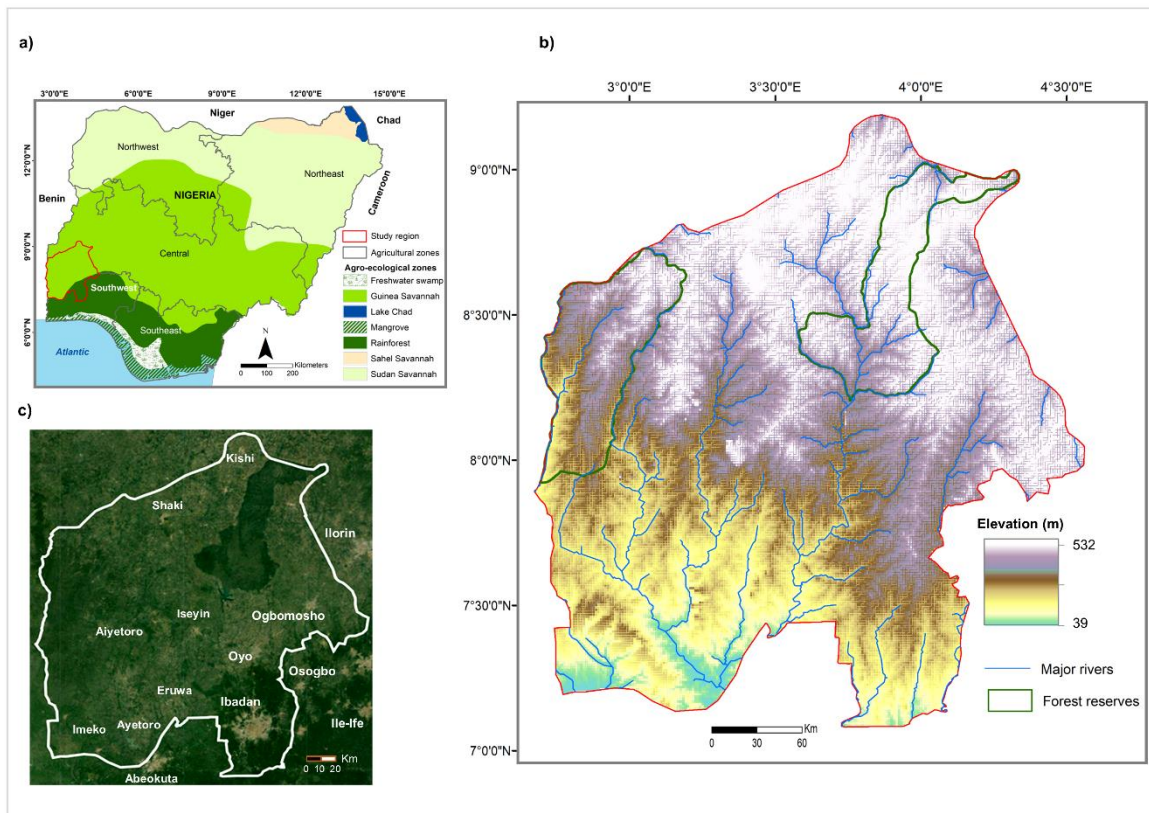
### 146 **2.1 Study region**

147

148 As the most populated African country, Nigeria is experiencing a food crisis with 17 million  
149 people estimated to be critically food insecure in 2022 due to natural disasters and social  
150 conflicts (Bizikova et al., 2022; Famine Early Warning System Network, 2023a, 2023b). The  
151 country comprises several agroecological zones (Fig. 1a). In the ultra-humid mangrove,  
152 freshwater swamps and rainforests, rainfall exceeds 2,000 mm yr<sup>-1</sup> and monthly min/max  
153 temperature (tmin/tmax) is 23/33°C. In contrast, the Guinea Savannah has ca.1,000 mm yr<sup>-1</sup>  
154 rainfall and monthly tmin/tmax of 20/37°C, the Sudan Savannah and Sahel Savannah are  
155 limited to 440 – 600 mm yr<sup>-1</sup> rainfall and tmin/tmax of 13 – 40°C (Iloeje, 2001). Agriculture in  
156 Nigeria is organized into five zones, these are northwest, northeast, central, southwest and  
157 southeast. LGS (our study region) falls mainly in the lower Guinea Savannah of the southwest  
158 agricultural zone. Elevation peaks at 532 m (Fig. 1b). There are two growing seasons in LGS,  
159 these are the early planting season and the late planting season. The early planting season



160 commences in March when rainfall starts, lasting until July. The late planting season begins in  
161 August and continues until rainfall cessation in October or November.



162  
163 Fig. 1. Study location a) The lower Guinea savannah in the Nigerian southwest agricultural  
164 zone, b) Biophysical context of the study region (Data source: Elevation – USGS 30 arc-second  
165 GTOPO30, rivers - FAO rivers in Africa, forest reserve boundaries - Protectedplanet), c)  
166 Depicting major settlements in the study region on a natural colour composite (Google Earth  
167 Engine 2022).  
168

169 Major farming systems that were identified as essential to meet the domestic food  
170 requirement are maize, cassava, yam and rice. Some minority crops were also considered (e.g.,  
171 cocoyam, sweet potato, cowpea). Table 1 shows the cropping calendar for these crops in 2022  
172 when fieldwork was conducted. To better capture the two growing cycles in our modelling for  
173 2022, we categorized maize and cassava into early and late planting. With the possibility that a  
174 field is cultivated during both planting seasons, the crop grown during each growing cycle is  
175 mapped and referred to as early maize, late maize, early cassava and late cassava. It is also  
176 possible that what was detected on the field during the early planting season was late cassava

177 planted the previous year during the early planting season. Such late cassava planted during the  
 178 last year is harvested after rainfall starts during the early planting season of the subsequent year.

179 Table 1. Cropping calendar for crops in eight farming systems in 2022

| Farming system                              | Mar | Apr | May | Jun | Jul | Aug | Sep | Oct | Nov | Dec | Jan | Feb |
|---|-----|-----|-----|-----|-----|-----|-----|-----|-----|-----|-----|-----|
| Early maize                                 |     |     |     |     |     |     |     |     |     |     |     |     |
| Late maize                                  |     |     |     |     |     |     |     |     |     |     |     |     |
| Early cassava                               |     |     |     |     |     |     |     |     |     |     |     |     |
| Late cassava                                |     |     |     |     |     |     |     |     |     |     |     |     |
| Yam   |     |     |     |     |     |     |     |     |     |     |     |     |
| Rice  |     |     |     |     |     |     |     |     |     |     |     |     |
| *Early maize –<br>Early cassava             |     |     |     |     |     |     |     |     |     |     |     |     |
| Others<br>Cocoyam<br>Sweet potato<br>Cowpea |     |     |     |     |     |     |     |     |     |     |     |     |

Sowing
Peaking /  
Maturing
Harvest  
period
2<sup>nd</sup>  
crop  
introduced
\*\*Multiple crops on farm

180 Note: \*The remains of the maize stems that were left standing after harvest in cassava fields  
 181 indicate maize-cassava mixed farming systems. \*\*The critical windows in the intercropping  
 182 system, whereby both crops are present on the field, must be detected to profile the crop  
 183 phenology properly. Information sources: oral interviews with Agricultural Development  
 184 Programme officials, farmers and the USDA crop calendar for Nigeria  
 185 [<http://fas.usda.gov/pecad/pecad.html> Accessed 09 March 2023]

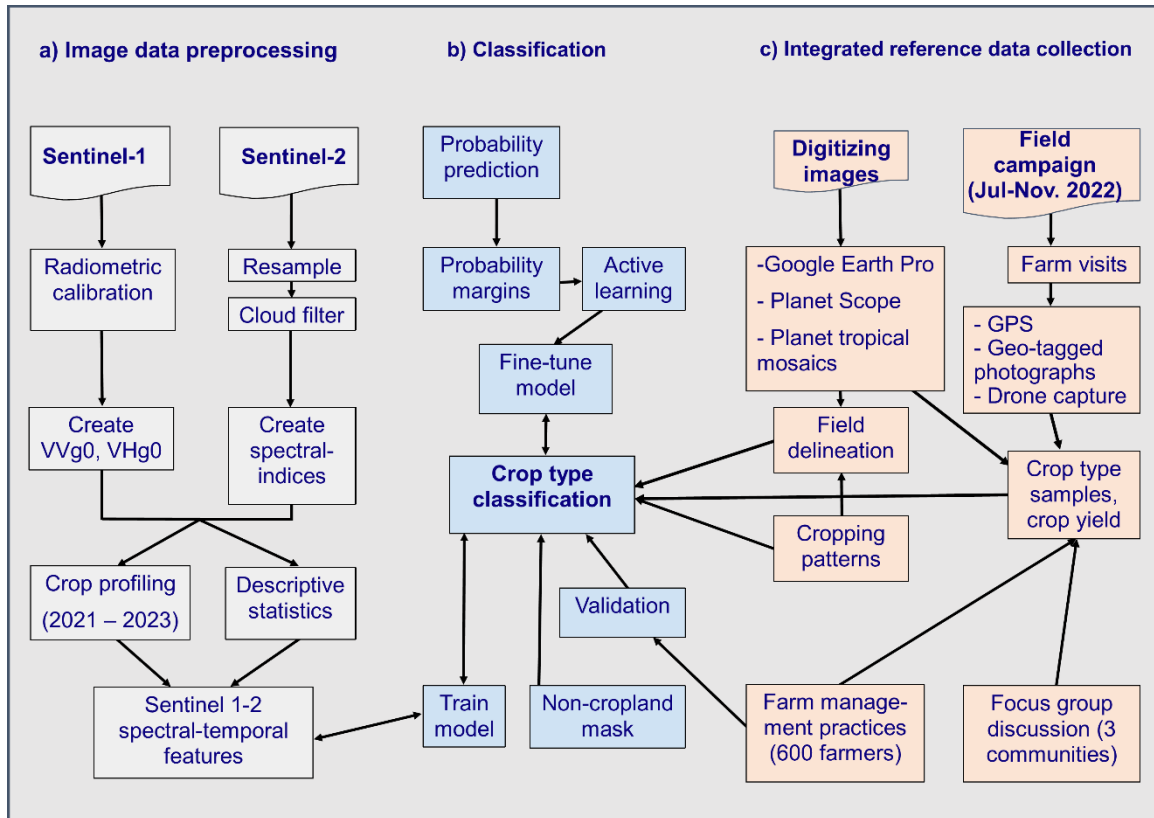
## 186 2.2 Mapping of farming systems

### 187 2.2.1 Workflow

188 The workflow comprises three main components (Fig. 2): a) A satellite remote sensing-based  
 189 image data preprocessing framework to create consistent spectral-temporal features of S1 and  
 190 S2 for mapping multiple crops and intercropping, b) model parameterization, classification,



191 iterative active learning to fine-tune model and k-fold cross validation, c) the reference data  
 192 collection used for model training and iterative active learning. The entire workflow was  
 193 developed in the Google Earth Engine Python Application Programming Interface (API)  
 194 (Gorelick et al. 2017).



195

196 Fig. 2. Workflow describing tasks in image preprocessing, crop type classification, and  
 197 reference data collection (remote sensing and place-based)

198

199

200 *2.2.2 Remote sensing data and preprocessing*

201

202 We used the S2A and S2B Level 2A image collection. All bands were resampled to 10m spatial

203 resolution. The Normalized Difference Vegetation Index (NDVI), Normalized Difference Bare

204 Index (NDBI) and the Normalized Difference Water Index (NDWI) were computed and

205 included in the classification. Due to the prevalence of cloud cover during the growing season,

206 we combined the S2 optical data with Synthetic Aperture Radar (SAR) data obtained from S1A.

207 We used the S1A C-band Ground Range Detected image collection, providing image data

208 which underwent thermal noise removal, radiometric calibration, and terrain correction using

209 the European Space Agency S1 toolbox. We retained only images from ascending orbit to  
 210 increase the consistency of the acquisition timing. We used the S1 Vertical transmit - Vertical  
 211 receive (VV) and Vertical transmit - Horizontal receive (VH) backscatter values to generate  
 212 VV gamma nought (VVg0) and VH gamma nought (VHg0) at 10m spatial resolution.

213 Both datasets were constrained to acquisitions between July 2021 and March 2023. The  
 214 S1 time series was aggregated into bins for the entire study period. In contrast, due to incessant  
 215 cloud cover during the rainy season, the S2 time series was constrained to the dry season, where  
 216 observation density is comparably high. We aggregated S1 and S2 into bins with varying sensor  
 217 constellations and temporal binning (Table 2). For each bin, we generated 25%, 50%, and 75%  
 218 percentiles, interquartile mean (imean), interquartile range (iqr), and standard deviation (sd) of  
 219 each band's surface reflectance or index values for S2. In contrast, for S1, we computed the  
 220 average VHg0 and VVg0 and cross-polarization ratio (CR) as the ratio between VHg0 and  
 221 VVg0 for each bin.

222

223 Table 2 Input features used for image classification experiments

| No. | Experiments                 | Number of features | S1        | S2        |
|-----|-----------------------------|--------------------|-----------|-----------|
| 1   | S1 bimonthly                | 27                 | bimonthly |           |
| 2   | S2 bimonthly                | 396                |           | bimonthly |
| 3   | S1 monthly                  | 54                 | monthly   |           |
| 4   | S2 monthly                  | 792                |           | monthly   |
| 5   | S1 monthly + S2 monthly     | 846                | monthly   | monthly   |
| 6   | S1 bimonthly + S2 bimonthly | 423                | bimonthly | bimonthly |
| 7   | S1 monthly + S2 bimonthly   | 450                | monthly   | bimonthly |

224

225

### 226 2.2.3 Reference data

227

228 Reference datasets required for model training and map accuracy assessment were acquired

229 during field campaigns from July to November 2022. We used a stratified random sampling

230 design to collect georeferenced data on crop types and cropping patterns (i.e., mono- or mixed  
 231 cropping). The strata are maize, cassava, yam, rice, sweet potato, cocoyam, legume (e.g.,  
 232 cowpea, peanuts), maize-cassava, maize-legumes and horticulture (e.g., tomato, pepper and  
 233 vegetable). Georeferenced samples were collected in Oyo and Ogun states, including geotagged  
 234 photographs and Red, Green and Blue (RGB) images (2 cm) using an Unmanned Aerial Vehicle  
 235 (UAV). Additional samples of crop types were digitized from Maxar images in Google Earth  
 236 Pro. The Planet Tropical Normalized Analytic Monthly Monitoring Mosaics complimented  
 237 with Level 1 PlanetScope surface reflectance scenes (3m) were used to cross-check these  
 238 samples (Planet Team, 2022; Planet-Norway International Climate and Forests Initiative -  
 239 Planet-NICFI, 2023). The reference datasets were compiled in QGIS 3.26 and ArcGIS 10.8.  
 240 Digitized crop samples were used to augment the field data, especially for the yam and rice  
 241 classes.

242 Eight target farming system classes were defined, indicating crop types, mixtures, and  
 243 growing periods (Table 3). These classes were early maize, late maize, early cassava, late  
 244 cassava, maize-cassava, yam, rice, and Others combining three minor crops. For classification,  
 245 we used a stratified sample (n=996) of all samples (n=2,127) to reduce class imbalances.

246

247 **Table 3.** Farming systems and the number of samples in the model run before and after active  
 248 learning (see section 2.2.4)

249

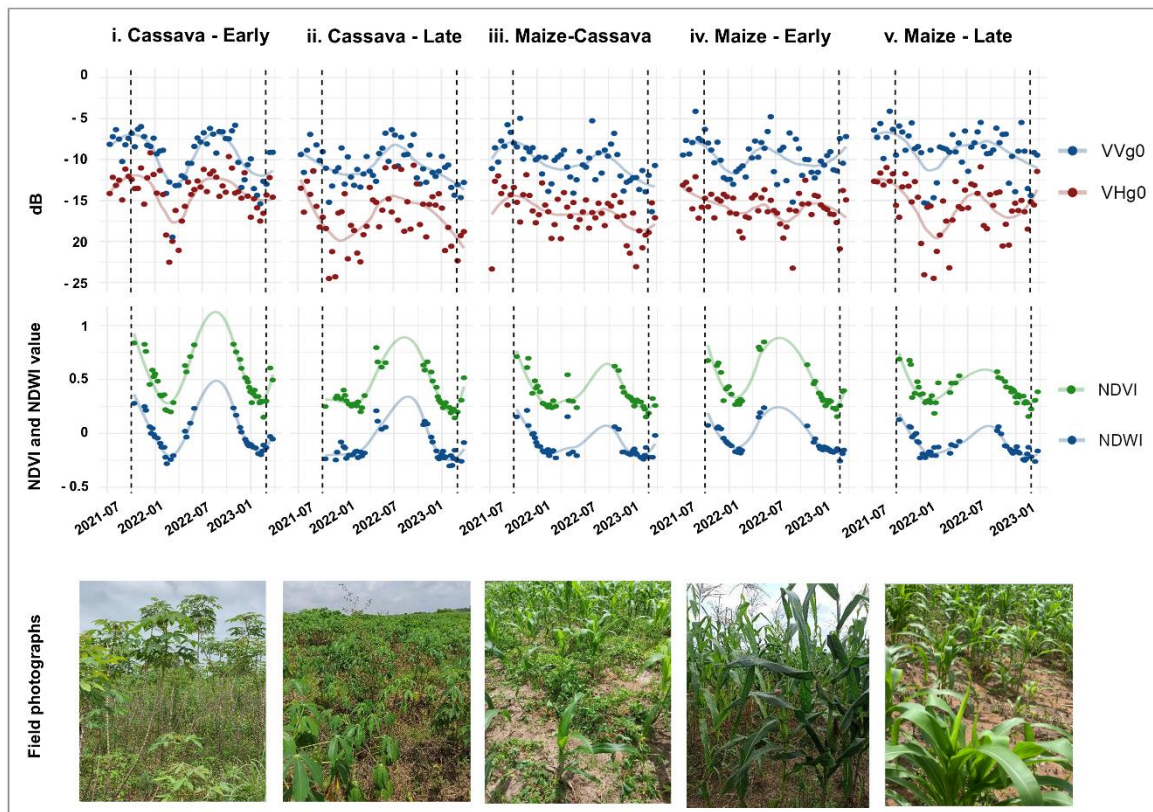
| <b>Farming system classes</b> | <b>Description</b>   | <b>Samples used</b> | <b>Active learning labels added</b> |
|-------------------------------|--|---------------------|-------------------------------------|
| Early maize                   | *Monocropping maize system planted in the early part of the first planting season. | 118                 | 8                                   |
| Late maize                    | **Monocropping maize system planted late during the second planting season.        | 99                  | 41                                  |
| Early cassava                 | Monocropping system of cassava planted during the first planting season.           | 171                 | 16                                  |
| Late cassava                  | Monocropping system of cassava planted late during the second planting season.     | 132                 | 6                                   |

|               |   |            |            |
|---------------|---|------------|------------|
| Yam           | Monocropping yam system, not including cocoyam.   | 167        | 41         |
| Rice          | Monocropping lowland rice grown on floodplains.   | 88         | 7          |
| Maize-Cassava | The mixed farming system of early maize is intercropped with early cassava. ***Cassava is introduced one month after planting maize. Maize is harvested before the canopy closure of cassava. | 151        | 29         |
| Others        | Cocoyam, sweet potato and cowpea.   | 70         | 0          |
| <b>Total</b>  |   | <b>996</b> | <b>148</b> |

250 \* The first planting season is from March to July. \*\*The second planting season is from August to October.

251 \*\*\*Farmers' description of their crop management practices.

252 We screened reference data by creating crop phenological profiles to aid in discriminating the  
253 identified farming systems from S1 and S2 images. Crop growth dynamics were inspected over  
254 time across multiple growing seasons from July 2021 to March 2023. This period was selected  
255 to better capture perennial crops (e.g., cassava) (Fig. 3). Crop profiles were created using S1  
256 time series of VHg0 and VVg0, vegetation (e.g., NDVI), bare (e.g., NDBI) and moisture indices  
257 (e.g., NDWI) were created from S2 time series. Image availability per sensor is the data point  
258 in the graphs (Fig. 3). The availability of S2 images was limited during much of the growing  
259 seasons (i.e., March - October 2022) due to cloud cover and shadow. This screening aided in  
260 assessing the quality of the samples for each farming system class, especially where information  
261 on vegetation presence was needed to discriminate early cassava from maize-cassava class.



262

263 Fig 3. Crop profiling based on S1 and S2 time series. Valid observations were interpolated using  
 264 locally weighted regression estimates (loess) to aid visual interpretation of phenological  
 265 profiles.

266

#### 267 2.2.4 Crop type classification

268

269 Crop type classification consisted of model training, iterative active learning to improve model

270 performance, and predicting the farming system classes throughout the study region (Fig. 2b).

271 We used the screened crop type samples to train the Random Forest model. Active learning was

272 also conducted to fine-tune the model (Tuai et al., 2011; Strumpf et al., 2014; Rufin et al., 2022).

273 Additional samples needed for active learning were created in areas of model uncertainty. Based

274 on the level of model uncertainty, we generated a map of probability margins from the Random

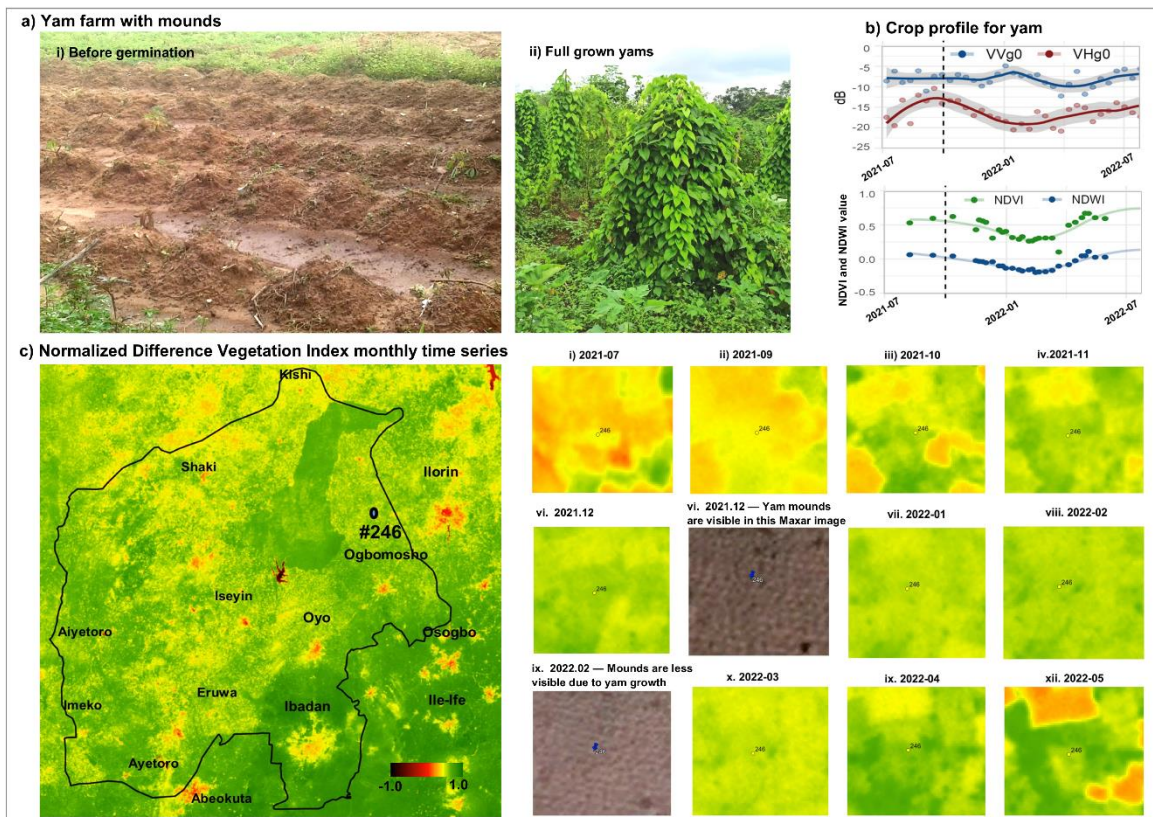
275 Forest class probabilities for the eight farming system classes (Fig. 2b). Probability margins

276 represent the probability difference between the predicted class and the class with the second-

277 highest probability value. Low probability margins indicate regions where the model is

278 uncertain and can profit from additional training samples. We calculated class-wise 25%  
 279 percentiles of probability margins and created a stratified random sample in the study area  
 280 (n=60 per class). To avoid sampling isolated pixels, we performed a sieving operation to sample  
 281 only from uncertain regions covering multiple pixels. Based on a qualitative assessment, we  
 282 tested different sieve sizes. We determined that a minimum size of six pixels provided the best  
 283 trade-off between maintaining small patches and avoiding sampling isolated pixels.

284 Once samples for active learning were generated, we identified the crop types and  
 285 appropriately labelled the samples (Fig. 4). First, we confirmed that the site was indeed  
 286 farmland by cross-checking with field data, including from UAV and very high resolution  
 287 satellite images. We then repeated the crop profiling step in 2.2.3 (refer to Fig. 4b). Lastly, to  
 288 determine the crop type, we examined the crop growth pattern using the PlanetScope monthly  
 289 NDVI Tropical Mosaics and multispectral images. These steps are demonstrated in Figure 4  
 290 using the example of a single pixel in the yam class.





293 Fig. 4. The procedure used to identify crop types for active learning samples, example of a yam  
294 farm (#246), a) The appearance of yam with the mounds varies widely depending on the stage  
295 of crop growth (i-ii), b) Crop profile, c) PlanetScope NDVI of May 2022 over the study area,  
296 d) Crop growth dynamics of #246 during different phenological stages are depicted in the  
297 monthly NDVI time series and very high resolution Maxar images (Google Earth image 2023  
298 Maxar Technologies).

299  
300         Due to the complex nature of our class catalogue, we identified additional labels for 148  
301 samples in uncertain areas, mainly for the yam and late maize classes. We discarded doubtful  
302 samples to avoid introducing other uncertainties to the model. Based on the complemented sets  
303 of reference data (n=1,144), we fine-tuned the trained random forest model for prediction and  
304 obtained the final map of farming systems in LGS. We based our classification of farming  
305 systems on Random Forest models using 250 trees (Breiman et al. 2001) as implemented in  
306 Google Earth Engine. This study used a Random forest classifier due to its proven performance  
307 in mapping crop types and heterogeneous landscapes. Studies applying random forest  
308 classifiers for crop-type mapping in African smallholder contexts include Nigeria (Ibrahim et  
309 al., 2021; Abubakar et al., 2023), Mali (Lambert et al., 2018), Kenya (Jin et al., 2019), South  
310 Africa (Mazarire et al., 2020). As a nonparametric classifier, Random Forest is considered  
311 suitable as the assumption of a normal distributed dataset is relaxed, does not require the use of  
312 statistical parameterization for class separation and overcomes the problem of overfitting (Sothe  
313 et al., 2017; Ouzemou et al., 2018).

#### 314 315 *2.2.5 Cropland masking*

316  
317 Constraining our farming system classification to cropland pixels required a suitable cropland  
318 mask. Therefore, we visually inspected multiple global and continental scale land cover  
319 products for their ability to accurately discriminate cropland from non-cropland in our study  
320 region. We here considered the 10 m resolution ESRI land cover (ESRI, 2023), ESA  
321 WorldCover 2021 (ESA, 2023) and MODIS land cover (Menashe and Friedl, 2018). The  
322 timeliness and spatial resolution made these products suitable candidates for cropland masking



323 in LGS. However, most products performed weakly in areas with a high presence of perennial  
324 crops with a high share of woody biomass (e.g., yam and cassava with stems of up to 1.5 m).

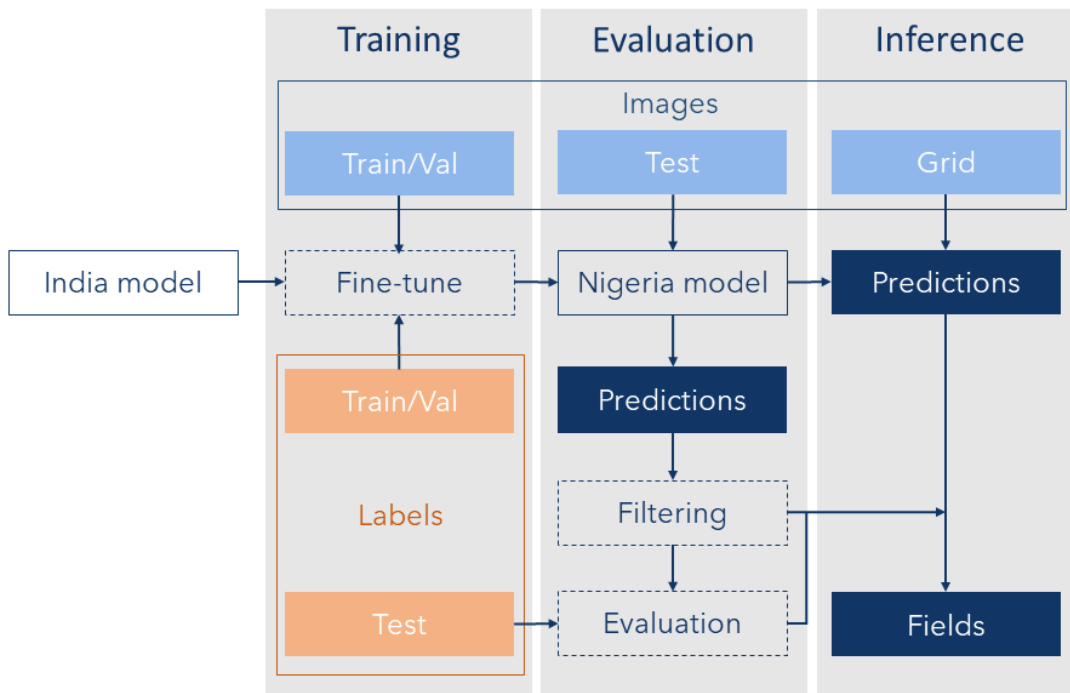
325 After careful evaluation, we used the WorldCover to mask out non-croplands from our  
326 study region. At 10m spatial resolution, the WorldCover matches our study period relatively  
327 well compared to other products available only for earlier years. We combined cropland,  
328 grassland and shrubland to avoid the erroneous removal of full-grown cassava and yam fields,  
329 especially in the northern parts of our study region.

### 330 *2.2.6 Validation*

331  
332 We conducted k-fold cross-validation using the reference datasets but excluded the active  
333 learning samples. Without wall-to-wall ancillary data that would enable us to generate labels  
334 for a random sample, it was not feasible to perform an area-adjusted accuracy assessment  
335 (Olofsson et al., 2014). We split our reference data into k=30 groups, iteratively trained Random  
336 Forest models with k-1 groups, and then predicted the farming system classes for the held-out  
337 sample (n=33). We compared predictions with field data and calculated Overall Accuracy  
338 (OA), User Accuracy (UA) and Producer Accuracy (PA) for all eight classes in each fold.

## 339 **2.3 Field delineation and field size estimation based on deep learning**

340  
341 We further examined whether field size is related to crop type and cropping patterns. We used  
342 a deep learning workflow relying on a ResUNet with pre-trained model weights from  
343 smallholder farming in India (Wang et al., 2022) and sub-meter imagery in Google Earth Pro™  
344 to delineate individual fields for 2,333 sites distributed across the study region (Fig. 5).



345

346 Fig 5. Workflow for field delineation. Val = validation.

347 *2.3.1 Image data and labels*

348 We created a stratified random sample ( $n = 500$ ) for model training in cropland regions. Using  
 349 very high resolution images from Google Earth Pro™, we screened individual images for  
 350 cropland presence and sufficient visibility of field boundaries. We generated a systematic  
 351 sampling grid with a three km distance to predict field size across the study region. This grid  
 352 was selected as optimal after evaluation with several grid sizes. We manually digitized all fields  
 353 for the images meeting these requirements ( $n = 293$ ), yielding 7,682 polygons representing  
 354 various field sizes and cropping patterns.

355 Field sizes in the reference data ranged between 0.01 ha and 59.52 ha (mean of 0.93 ha,  
 356 standard deviation of 1.69 ha). We divided this digitized field data into training (60%),  
 357 validation (20%) and test data (20%). We used the polygons to create multi-task labels in raster  
 358 format representing three layers: 1) a binary layer indicating the presence of a crop field, 2) a  
 359 binary layer indicating the presence of a field boundary and 3) a continuous layer representing  
 360 the normalized distance of each field pixel to the nearest field boundary. We removed points

361 with less than 10% cropland in its surrounding area (36 ha), according to the WorldCover 2021  
362 cropland mask. A total of 2,333 sites were returned, which were then used to delineate  
363 individual fields and estimate field size at the field, local, and regional levels.

364

### 365 *2.3.2 Model training, filtering and evaluation*

366 We used the image data and labels to fine-tune a FracTAL ResUNet, a state-of-the-art model  
367 architecture designed to delineate agricultural fields (Waldner et al., 2021). We obtained pre-  
368 trained model weights from Wang et al. (2022) and fine-tuned the model for 50 epochs using a  
369 batch size of four, a learning rate of 0.0005 and the Adam optimizer (Kingma and Ba 2014).

370 Our study region's agricultural landscape complexity and diversity challenged the  
371 production of accurate field delineations. For some sites, non-cropland patches (e.g., short  
372 fallows or clusters of dense shrubs) were falsely detected as a crop field, which can, in the  
373 absence of a sufficiently detailed cropland mask, introduce biases in field size estimates. We  
374 noted that in these cases, prediction confidence reflected comparatively lower scores. We,  
375 therefore, constrained the analyses to fields predicted with high confidence by introducing  
376 filtering based on prediction confidence. We first removed incomplete fields in each site  
377 because correct field size estimates cannot be obtained from fields extending beyond the  
378 predicted image. We then filtered predicted fields (i.e., model delineated fields) based on the  
379 prediction confidence, a score derived as the median predicted probability of all pixels within  
380 a field being cropland with probabilities of 0 to 1. We conducted sensitivity analyses to obtain  
381 the optimal thresholds for filtering field predictions by testing six threshold values between 0.70  
382 and 0.95 in steps of 0.05 (i.e., 0.70, 0.75, 0.80, 0.85, 0.90 and 0.95).

383 We evaluated the model performance based on predictions of the test split (n = 62 sites)  
384 to assess the suitability of the predictions at the field and site levels. We assessed field-level  
385 spatial agreement based on mean intersection over union (mean IoU), the fraction of fields with

386 IoU scores above 0.80 and field-level precision and recall. At the site level, we assessed the  
387 agreement in field size estimates using root mean squared error (RMSE), mean absolute error  
388 (MAE), and mean error (ME) in hectares and relative mean absolute error (relative MAE),  
389 expressing the error in relation to observed field size. We then calculated the weighted mean  
390 field size estimates. The weighting of the mean field size estimate accounts for the higher  
391 relevance of large fields when calculating the field size at the site level. We conducted  
392 sensitivity analyses to identify a good balance between error metrics, high spatial agreement,  
393 and site-level field size estimation by evaluating the performance across the six confidence  
394 filtering thresholds.

### 395 *2.3.3 Linking field size and farming systems*

396 We used the predicted samples of the 2,333 sites, removed incomplete field predictions, and  
397 filtered based on the confidence threshold obtained from the sensitivity analyses. For the  
398 resulting fields, we aggregated our farming system map to the field-level based on the majority  
399 class present in each field. Moreover, we estimated the weighted mean field size at the site-  
400 level to assess the spatial distribution of field size in the study region. For better interpretation,  
401 we categorized field sizes into five classes representing very small (0.00-0.25 ha), small (0.25-  
402 0.50 ha), medium (0.50-1.00), large (1.00-2.50 ha), and very large (2.50-10.00 ha) fields.

## 403 **3. Results**

### 404 **3.1. Mapping heterogeneous farming systems**

#### 405 *3.1.1 Accuracy assessment*

406  
407 We assessed the mean overall accuracy and the observed standard deviation in the k-fold cross-  
408 validation across all single-sensor and multi-sensor experiments with bimonthly and monthly  
409 temporal bins (Table 4). All experiments involving S2 (i.e., experiments 2, 4, 5, 6, 7) yielded  
410 overall accuracies above 0.76, whereas experiments involving only S1 (i.e., experiments 1 and  
411 3) did not perform well with overall mean accuracies of 0.50. The highest mean overall

412 accuracy of 0.79 (+/- 0.09) and 0.78 (+/- 0.10) were obtained in experiment 5 (combining  
413 monthly S1 and monthly S2 spectral features) and experiment 4 (monthly S2), respectively.  
414 However, the maps based on the monthly S2 features alone (i.e., experiments 4 and 5) had a  
415 high share of data gaps due to clouds (Fig. 6), which affected 10.2% of the cropland area.  
416 Therefore, we decided to base our analyses on the map from experiment 7 (i.e., S1 monthly and  
417 S2 bimonthly data), despite the slightly lower mean overall accuracy of 0.77 (+/- 0.08), as it  
418 effectively reduced the fraction of data gaps to 0.2%.

419

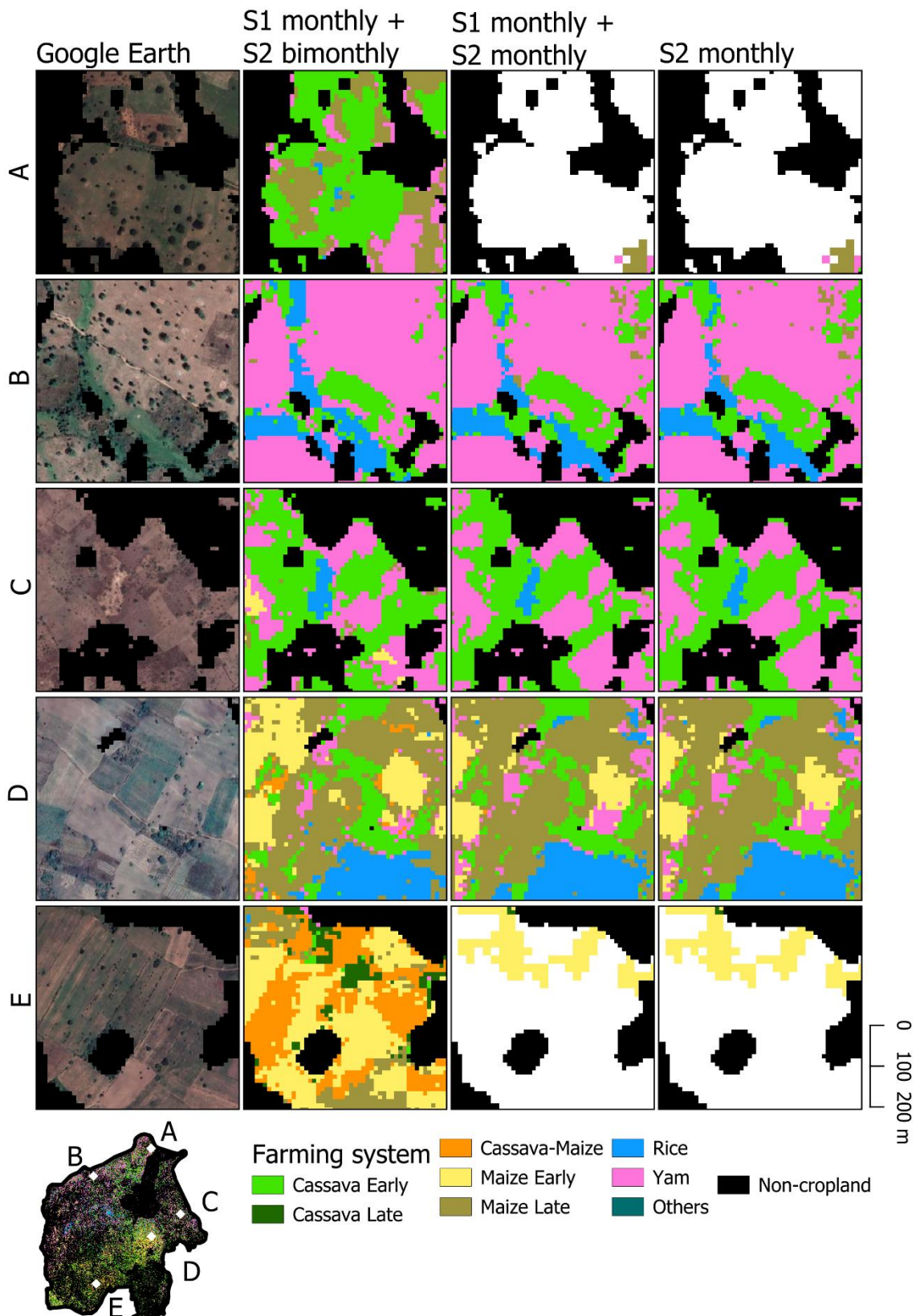
420 Table 4 Overall accuracies across experiments with reported features, mean overall accuracy,  
421 standard deviation, and standard error of the mean estimate. Scores were derived from 30-fold  
422 cross-validation.

423

424

425

| No. | Experiments                 | mean overall accuracy | standard deviation | standard error |
|-----|-----------------------------|-----------------------|--------------------|----------------|
| 1   | S1 bimonthly                | 0.50                  | 0.10               | 0.02           |
| 2   | S2 bimonthly                | 0.76                  | 0.08               | 0.01           |
| 3   | S1 monthly                  | 0.50                  | 0.08               | 0.02           |
| 4   | S2 monthly                  | 0.78                  | 0.10               | 0.02           |
| 5   | S1 monthly + S2 monthly     | 0.79                  | 0.09               | 0.02           |
| 6   | S1 bimonthly + S2 bimonthly | 0.76                  | 0.07               | 0.01           |
| 7   | S1 monthly + S2 bimonthly   | 0.77                  | 0.08               | 0.01           |



429  
430  
431  
432  
433

Fig 6: Comparison of Google Earth VHR imagery and three map versions (columns) integrating S1 monthly and S2 bimonthly, S1 and S2 monthly and only S2 at monthly intervals across different parts of the study region (rows). Black pixels indicate non-cropland, and white pixels indicate data gaps, according to WorldCover 2021.

434 The selected model based on monthly S1 and bimonthly S2 features (experiment 7) yielded  
 435 high class-specific accuracies, yet with substantial variation across the 30 folds (Fig. 7). Mean  
 436 user accuracies exceeded 0.70 for all classes, with standard deviations ranging between 0.19  
 437 (yam) and 0.32 (Others). The highest mean user accuracies were reached for rice (0.90 +/- 0.18),  
 438 early maize (0.81 +/- 0.22) and maize-cassava (0.79 +/- 0.20). The lowest user accuracies were  
 439 for late cassava (0.71 +/- 0.23) and late maize (0.74 +/- 0.27). Mean producer accuracies were  
 440 particularly high for early maize (0.89 +/- 0.22), maize-cassava (0.85 +/- 0.19), and yam (0.85  
 441 +/- 0.19). The lowest mean producer accuracies occurred for late maize (0.58 +/- 0.26) and  
 442 Others (0.71 +/- 0.31).



443

444 Fig. 7: Class-wise PA (top) and UA (bottom). Scores derived from 30-fold cross-validation.  
 445 Horizontal lines represent the median score, whereas the points are the mean scores.

446

447

448

449

450

451

452



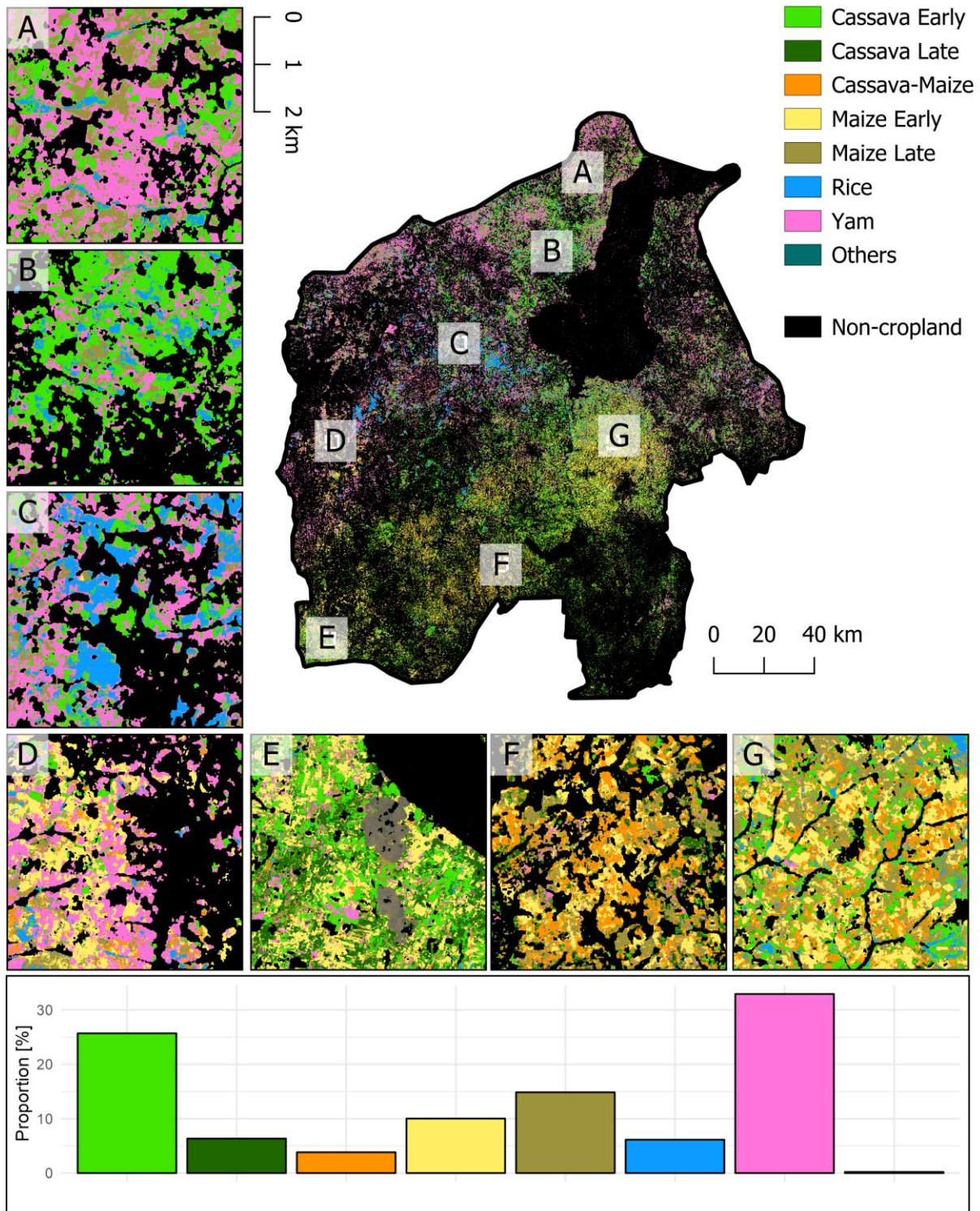
453 3.1.2 Spatial patterns of major farming systems

454

455 We mapped the distribution of the eight major farming systems in the LGS. We considered

456 maize, cassava, yam, rice, mixtures of maize-cassava and the Others class (i.e., cocoyam,

457 cowpea and sweet potatoes) during the 2022 early and late planting seasons (Fig. 8).



458

459 Fig. 8: A-G show close-ups of classification results. A) major yam growing areas near Kishi  
460 and Shaki, B) early cassava area near Igboho, C) Lowland rice cultivation in the Igbeti area, D)  
461 early and late maize in the Aiyetoro area of Oyo state, E) early and late cassava with early maize  
462 near Imeko, F) maize-cassava intercropping in Aborisade near Eruwa, G) late maize and maize-  
463 cassava intercropping in the Ogbomosho area (Refer to Fig. 1c for the locations of these  
464 settlements). The bar chart depicts the proportion of fields contained in each farming systems.

465  
466  
467

468 Although different parts of the LGS specialized in certain crops, yam is widely grown across  
469 the region. Overall, the distribution of the farming systems across croplands in the study region  
470 was as follows: early cassava: 25.7%, late cassava: 6.3%, maize-cassava: 3.8%, early maize:  
471 10.0%, late maize: 14.9%, rice: 6.1%, yam: 32.9%, and Others: 0.2% (Figure 9)

472

## 473 3.2 Field size analyses

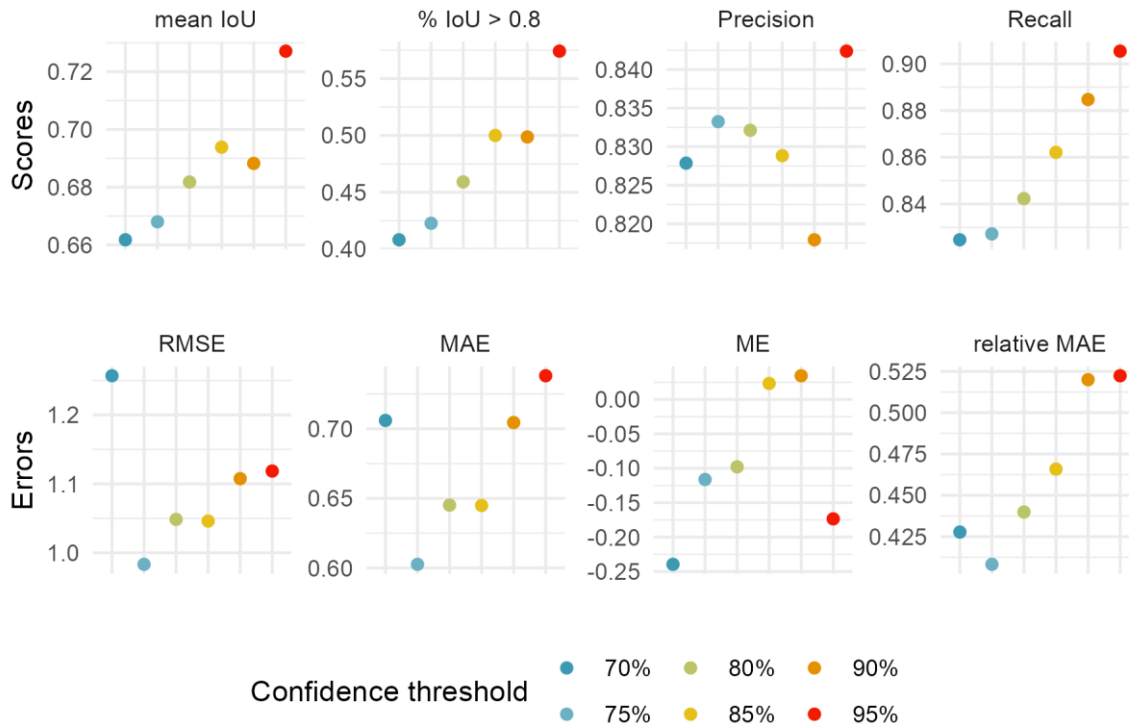
474

### 475 3.2.1 Automated field delineation performance

476

477 The evaluation of the field delineation revealed high field-level agreement with mean IoU  
478 scores ranging between 0.66 for the 70% and 0.73 for the 95% confidence thresholds (Fig. 9).  
479 For all confidence thresholds of 85% and above, at least half of the fields had mean IoU scores  
480 of 0.8 or higher. Good balance in precision and recall was achieved at 95% and 85% confidence  
481 thresholds, respectively. Field size estimates at the site level had the lowest RMSE (0.983 ha)  
482 and MAE (0.603 ha) when using 75% confidence thresholds. However, ME (i.e., bias) was  
483 lowest (0.023 ha) at 85% (46.5%), whereas MAE at 75% was 40.8%. Due to the high level of  
484 spatial agreement and the overall low bias in field size estimates, we decided to use the 85%  
485 confidence threshold for filtering the predictions across the sample grid.

486



487  
 488 Fig. 9: Evaluation of field-level spatial agreement (top row) and site-level field size estimation  
 489 (bottom row) based on test split (n sites =62) across confidence thresholds used for filtering.  
 490

491  
 492 *3.2.2 Field size distribution*  
 493

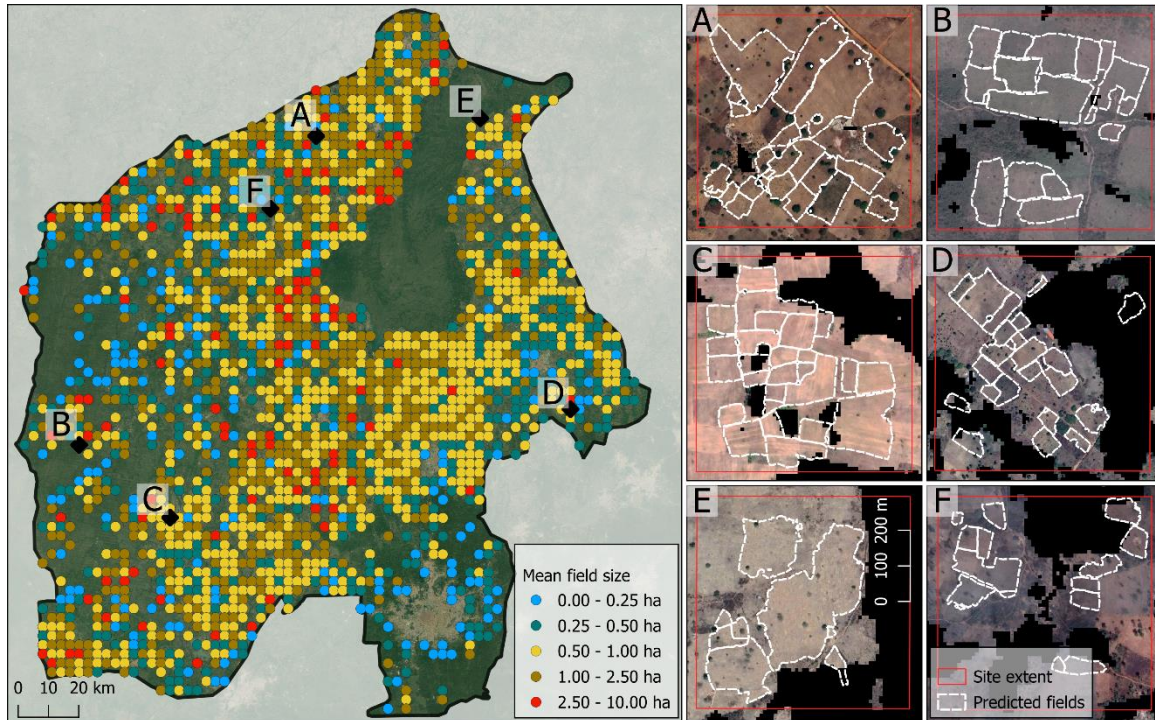
494 We assess the distribution of mean field sizes across the study region based on the sample grid  
 495 at three km distance (Fig. 10). With a mean field size of 0.6 ha, we observed a dominance of  
 496 medium field sizes (0.50-1.00 ha), which clustered across large parts of the study region. Both  
 497 medium and large (1.00 - 2.50 ha) field sizes were prevalent at the site level, while very large  
 498 (2.50 - 10.00 ha) field sizes were scattered and comparatively rare. Very small (< 0.25 ha) and  
 499 small (0.25 - 0.50 ha) fields were mainly found in the more fragmented landscapes in the  
 500 southeastern and western parts of the study region, where the share of agricultural land is  
 501 comparatively low and natural vegetation persists. Differences in field sizes ranged from larger  
 502 fields in the North, where yam and cassava are predominantly grown, to smaller fields in the  
 503 southern region. Larger monocropping fields, especially for yam, were more in the northern  
 504 part of our study area, whereas much smaller and heterogenous fields to the South. The  
 505 southeastern parts include the urban environment around Ibadan, which is transitioning into the



506 rainforest ecosystem and is thus dominated by forests. The western and northern section of the  
507 study region is characterized by savanna vegetation.

508

509



510  
511 Fig. 10: Spatial distribution of mean field size (left) and examples of field predictions filtered  
512 using the 85% confidence threshold (A-F).

513

514

### 515 3.2.3 Relating field sizes to farming systems

516

517 We intersected the model-delineated fields with the farming system map to explore field size

518 distribution across the different farming systems. Filtering the model-delineated fields in all

519 2,333 sites using the 85% confidence threshold resulted in 14,000 fields with a size ranging

520 between 0.001 ha and 9.9 ha. We then intersected this field size output with our farming system

521 map and assigned the majority farming system to each model-delineated field.

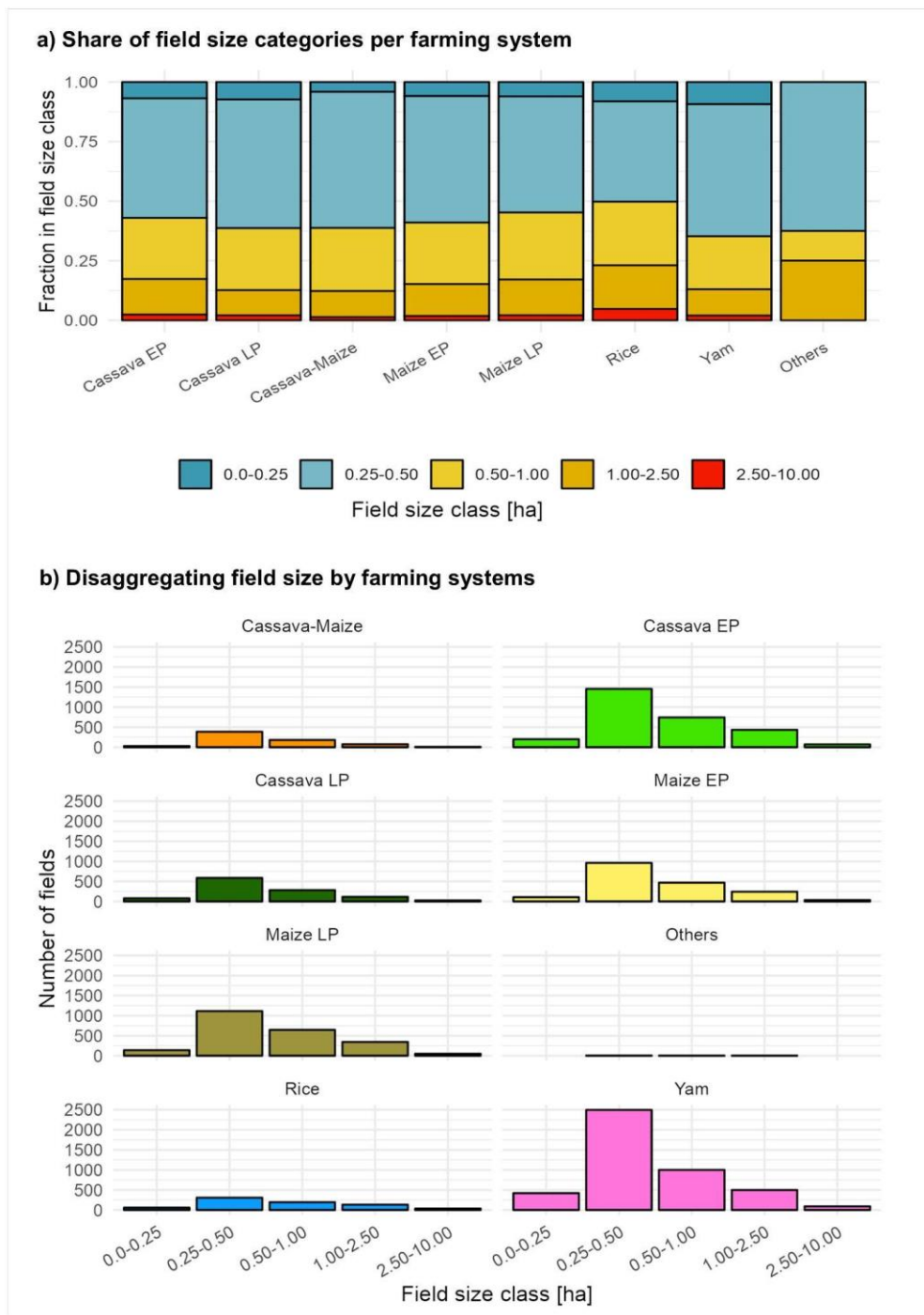
522 Relating field size to farming systems, the region was dominated by small fields (52.2%)

523 and medium-sized fields (25.1%), followed by large (13.2%), very small (7.4%), and very large

524 fields (2.2%). On average, the mean field size was 0.6 ha. Stratifying across farming system

525 classes, medium to larger fields (>0.5 ha) were more frequent for early cassava, late maize and

526 rice (Fig. 11a). A stratification of farming systems and field size revealed a similar distribution  
 527 of field size categories across the farming systems (Fig 11b).



528 Figure 11 Relating field size categories to farming systems. a) Relative share of field size class  
 529 per farming system, b) Histograms relating field size categories to farming systems  
 530  
 531

532 Maize-cassava and late cassava showed lower shares of large and very fields. The number of  
 533 fields present for each farming system reflects the overall proportions of the mapped farming

534 systems. As such, only a few fields of the Others class were included in this analysis. Fields  
535 below 0.25 ha were comparatively rare in the study region, but fields of 0.25 - 0.50 ha  
536 dominated all farming systems.

## 537 **4 Discussion**

538

### 539 **4.1 Spectral-temporal metrics from Sentinel 1 and Sentinel 2**

540 The smallholder agricultural settings we studied fall within the lower Guinea Savannah of  
541 southwest Nigeria. As in many parts of the tropics, the region is characterized by incessant  
542 cloud cover. Clouds and associated shadows critically challenge the use of optical sensors  
543 (Whitcraft et al., 2015; Danso et al., 2019). Hence, the temporal frequency of usable S2 images,  
544 especially during the growing seasons, is drastically reduced. This necessitated using S1 radar  
545 data whose observations do not depend on solar illumination or atmospheric conditions  
546 (Khabbazan et al. 2019) in combination with S2, providing richer spectral information.

547 Our experiments returned lower overall accuracies of about 0.50 when only S1 features  
548 were used. Some studies (e.g., Kpienbaareh et al., 2021; Rao et al., 2021) confirm the  
549 inadequacy of S1 data for crop type mapping in smallholder contexts despite reports of better  
550 results in the range of 0.85 - 0.90 in other agricultural contexts and regions (e.g., Veloso et al.,  
551 2017; Vreugdenhil et al., 2018; Khabbazan et al., 2019; Planque et al. 2021). Veloso et al.  
552 (2017) demonstrated that S1 (particularly the VH/VV ratio) yielded valuable information on  
553 crop development after comparing fresh biomass, NDVI, precipitation and temperature to S1  
554 data. They noted the potential to distinguish between crops based on the temporal variation of  
555 backscatter, especially for barley and maize. Similarly, Planque et al. (2021) reported that S1  
556 backscatter and interferometry show a high consistency for crop monitoring and detecting key  
557 dates for important crops in the Netherlands. They highlighted that structural and biomass

558 changes associated with crop development influenced the backscatter for each crop class  
559 mapped throughout the season. These examples of achievements using S1 mainly relate to  
560 monocropping systems in developed countries, which are less complex than our smallholder  
561 setting.

562  
563 Further, our results improved to 0.78 using only S2, especially the monthly S2 features,  
564 despite cloud cover and related artefacts. This better result with S2 is in line with most studies  
565 on smallholder agriculture in Africa using only S2 for crop type mapping, such as in Nigeria  
566 (Ibrahim et al., 2021), Mali (Lambert et al., 2018), Kenya (Jin et al., 2019), and South Africa  
567 (Mazarire et al., 2020). However, the use of S2 features alone was precluded for our study  
568 region because of the lack of data in about 10% of the area studied. The non-availability of S2  
569 data within the critical temporal windows in the growing season is a limitation for crop type  
570 mapping in smallholder regions such as ours. The availability of cloud-free optical (S2)  
571 observations was essential in differentiating crop phenology and, ultimately, crop types (Frantz,  
572 2019), especially within the identified critical temporal windows for crop type differentiation  
573 and mapping (Griffiths et al., 2019; Ibrahim et al., 2021). Ibrahim et al. (2021) reported the  
574 importance of S2 spectral bands performing well when systematic narrow temporal critical  
575 windows are used in predicting intercropped classes.

## 576 **4.2 Mapping of multiple crops and intercropping**

577  
578 Most remote sensing studies do not account for intercropping and multiple growing cycles in  
579 classifying and predicting crop types (Jin et al., 2019; Ibrahim et al., 2021). To improve the  
580 identification of multiple crops, especially crops growing in intercropping systems, we screened  
581 our sample data (both field-based and from satellite imagery) for quality. The 3m PlanetScope  
582 images (i.e., multispectral and monthly NDVI) and 0.6m resolution Maxar images were most



583 helpful in confirming crop growth patterns in the crop profiles created with S1 and S2. Crop  
584 types were identified based on crop phenology from satellite imagery, geotagged pictures, and  
585 RGB imagery from UAV. Samples were discarded in areas where very high-resolution images  
586 were unavailable for the required date. We recommend better access to higher resolution images  
587 to meet the challenges of mapping the heterogeneous agricultural landscapes typical of  
588 smallholder farms. This decade (2019–2028) is the Decade of Family Farming (United Nations,  
589 2017), which is typical of most smallholder farms. However, not all smallholder farms are  
590 family farms (Lowder et al., 2021).

591         A novelty we present in this section is harnessing the monthly NDVI time series to  
592 visually identify spatio-temporal phenology stages to actively label different crop types, which  
593 can be applied in similar smallholder regions. Temporal characteristics of farming activities –  
594 field clearing, crop emergence, crop peaking and senescence stages – helped to identify and  
595 label different crop types, especially for the early and late planted maize classes, for which their  
596 growth stages in the early or late part of the growing season was most critical for identification.  
597 We considered it essential to capture intercropping as it is the dominant farming practice in  
598 smallholder farming systems, especially in Africa. Perception studies among smallholder  
599 farmers have found that farmers intercrop to forestall total crop failure. For example, drought  
600 is perceived to impact crops differently. Likewise, intercropping provides nutritional options,  
601 enables nitrogen fixation by legumes, and sometimes serves as a physical barrier to pests and  
602 diseases (Bouws and Finckh, 2008; Akinyemi, 2017; Kinyua et al., 2023).

603         From a remote sensing methods point-of-view, identifying and predicting crops in  
604 intercropping systems (e.g., maize-cassava) is particularly challenging because of the different  
605 sowing dates, similarity in the crops' comparable height and structure. Yam was the easiest to  
606 detect in our study region from very high resolution images due to its distinct ridges or mound  
607 patterns. However, full-grown yams are often spectrally similar to tree crops and shrubs in

608 smallholder farms. We found that yam occupied about 40% of the land area in our study region.  
609 The cassava class also exhibited a slight distinction in texture from the Others class. As cassava  
610 can grow more than 1.5m, it was difficult to distinguish it from tree crops and shrubs. The maize  
611 class was challenging to identify or improve using the active learning methodology, as it  
612 revealed no distinct pattern and texture across all growing stages. The rice class was identified  
613 well by its smooth texture and being associated with floodplains. Using field-based information  
614 about cropping patterns and crop management practices (e.g., crop sowing dates and sequence),  
615 we could label samples for all classes except mixtures using our active learning methodology.  
616 Identified crop mixture samples such as intercropping from very high resolution images were  
617 discarded as these were particularly doubtful considering the mixed crop signatures in the  
618 images and different growth stages of the crops. The overall pattern of monocropping fields of  
619 early cassava, late maize, rice and yam clustered mostly in the North, whereas intercropped  
620 fields of maize-cassava and monocropped late maize were mainly present in the fragmented  
621 agricultural landscapes in the South.

622 From an economic perspective, the study focused on identifying major farming systems  
623 for producing major food staples that are widely consumed locally to ensure their relevance in  
624 meeting the domestic food needs of the region and to infer feasible surpluses for export. For  
625 example, cassava is an economic crop that is processed locally into different food products.  
626 Cassava is equally important for local industry and export, e.g., for producing ethanol and  
627 cassava chips for battery production (Kolawole et al., 2010; Srivastava et al., 2023). Maize and  
628 cassava are two crops favoured for intercropping by farmers for economic reasons (Nwokoro  
629 et al., 2021; Kinyua et al., 2023). While cassava matures after 12 months, maize is fast  
630 growing and ready for harvest in 2.5 - 3 months – a so-called “hunger-combating crop”.  
631 Moreover, farmers in this and similar smallholder regions take advantage of the multiple  
632 growing cycles in the region to grow crops several times a year.

### 633 4.3 Relating field size to cropping systems

634  
635 We established the empirical relationship between field size and cropping systems in the  
636 smallholder farming systems of LGS. The first step was to detect individual fields at very high  
637 spatial resolution with Deep Transfer Learning and then to intersect delimited fields from the  
638 model with the farming system map. Deep learning segmentation of field size using automation  
639 algorithms is becoming an efficient tool for delineating field sizes (Waldner et al., 2020).  
640 However, these methods are challenged in smallholder regions with heterogeneous farming  
641 systems, often changing field borders or having no clear field borders (Samberg et al., 2016;  
642 Fatunbi et al., 2020). Irregular crop field patterns and sometimes drainage channels created  
643 within a farm complicate deciding where the boundary of one farm ends without very clear field  
644 demarcations or cadastre information. Despite these challenges in smallholder systems, Wang  
645 et al. (2022) demonstrated the robustness of the methodology we adopted for Indian smallholder  
646 settings. Similarly, we achieved high accuracy in extracting field outlines and deriving field  
647 size information.

648 Monocropping was positively related to larger field sizes in the LGS. From a historical  
649 perspective, Nigeria has pursued agricultural land expansion programmes requiring land to be  
650 converted to croplands, resulting in extensive forest clearing for agricultural purposes (Ekong,  
651 1983; Akinyemi, 2013; Akinyemi and Ifejika Speranza, 2022). Associated with the expansion  
652 of croplands was the structural change to smallholder agriculture, from a highly subsistence  
653 structure to commercial, which is reflected in changing field sizes. The spatial distribution of  
654 field size across the region reveals a mean field size of 0.60 ha with variations between different  
655 farming systems. Although the share of field size was dominated by small fields (52%) and  
656 medium-sized fields (25%), large to very large fields covered 15.4% of our study region. We  
657 question whether smallholder crop fields are still to be generalized at sizes of <2 to 5 ha for  
658 sub-Saharan Africa (FAO, 2015; Banerjee et al., 2015; Fritz et al., 2019). In our analysis of

659 field sizes, some fields were found within >1.0 to 10 ha thresholds. These thresholds are larger  
660 than the *very small* (<0.64 ha) and *small field* (0.64 - 2.56 ha) classifications where the majority  
661 (87%) of Nigeria's fields were captured, according to Lesiv et al. (2019). The occurrence of  
662 larger field sizes in our study region can be attributed to the emergence of *step-up farmers*, i.e.,  
663 smallholder farmers who expanded their farming operations from small to medium-sized fields  
664 and the influx of *step-in* farmers, i.e., diaspora investments in the agricultural sector associated  
665 with increasing agri-businesses (Chiaka et al., 2022). Chiaka et al. (2022) found a proportional  
666 increase in medium- and large-sized farms in Nigeria between 2015 and 2018. Jayne et al.  
667 (2022) found an increasing trend in the rise of medium-sized farms in seven African countries.  
668 They attributed the increase in field size to investor farmers and the policy efforts supporting  
669 agricultural transformation in Africa.

670

## 671 **5. Conclusions**

672 To our knowledge, a few examples demonstrate the opportunities of satellite remote sensing  
673 for mapping multiple crops and intercropping across multiple growing cycles. These are the  
674 critical gaps this study fills using as a case the complex and heterogeneous smallholder systems  
675 of the lower Guinea Savannah of Nigeria. Like most parts of sub-Saharan Africa, Nigeria lacks  
676 crop type maps even though they are baseline data for food security and planning. With the  
677 mapping complexities associated with smallholder agriculture, our results revealed the potential  
678 of combining optical and radar (e.g., S2 and S1) data. Better crop type prediction in  
679 heterogeneous farming systems, including intercropping and dual cropping cycles, was  
680 achieved, which was previously lacking in the literature. Different combinations of monthly  
681 and bimonthly S1 and S2 features achieved accuracies ranging from 76 to 79%, which are  
682 comparable to most monocropping and single cropping cycle studies. Like most previous

683 studies, our findings suggest improving the mapping accuracy with the combination of multiple  
684 sensors. Integrating the new Environmental Mapping and Analysis Program (EnMap)  
685 hyperspectral bands with S1 and S2 images may improve crop type mapping in smallholder  
686 agriculture despite mapping challenges. For example, the narrower spectral windows of the  
687 EnMap may provide critical spectral information for capturing crop mixtures in heterogeneous  
688 smallholder regions as they are currently not explored to our knowledge.

689 Our approach allowed us to define eight farming system classes indicating crop types,  
690 crop mixtures, and the planting period during the first planting season (i.e., early growing cycle)  
691 and the second (late growing cycle). We perceive room for improvement by separating crops  
692 combined in the Others class containing multiple crop types such as cocoyam, cowpea and  
693 sweet potato. As there might be omission errors in the Others class, separating crops in this  
694 class may provide a more robust outlook. We had spectral mixtures between yam and cassava  
695 with shrubs and tree crops, whether in mono- or intercropping farming systems. Consequently,  
696 this study did not consider tree crops to minimize the complexity of mapping mixed farming  
697 systems with Remote Sensing, especially when developing each crop's phenology and  
698 experimenting with combinations of S1 and S2 features. We now recommend explicit  
699 methodology for separating tree crops and perennial crops (e.g., yam and cassava) in future  
700 studies.

701 By mapping multiple crops and differentiating cropping patterns into mono- and  
702 intercropping using Remote Sensing and Machine Learning, the information provided in this  
703 study is valuable for future downstream assessments of crop production and yields and the  
704 inference of the influence of agricultural structural changes such as farm consolidation on crop  
705 production. We recommend adapting our methodology to produce wall-to-wall crop type maps  
706 for similar regions.

## 707 Acknowledgements

708 This research was conducted within the Land-use Change and the Resilience of Food  
709 Production Systems (LucFRes) project. This project has received funding from the European  
710 Union (EU) Horizon 2020 research and innovation programme under the Marie Skłodowska-  
711 Curie (grant agreement no. 101025259). The Women in Natural Sciences Award granted to Dr.  
712 Akinyemi by the Einstein Foundation and the Berlin University Alliance in 2023 is also  
713 gratefully acknowledged. Dr. Rufin was supported by the Fund for Scientific Research – Fonds  
714 de la Recherche Scientifique (grant agreement no. T.0154.21). We would like to thank the  
715 Agricultural Development Programme officials of the Ministry of Agriculture, Commodity  
716 farmers' associations, the communities visited, farmers for their time and for sharing valuable  
717 farm management practices, and the various local fieldwork team members whose names are  
718 too numerous to mention. We are also grateful for access to PlanetScope scenes and Tropical  
719 Mosaic images by Planet-NICFI and Planet's Education and Research Program. We appreciate  
720 the free and open access to Sentinel-1 and Sentinel-2 data and open cloud geospatial processing  
721 tools in Google Earth Engine. This study contributes to the Global Land Programme  
722 (<https://glp.earth>) and the Programme on Ecosystem Change and Society ([https://www.pecs-](https://www.pecs-science.org)  
723 [science.org](https://www.pecs-science.org)). All content and information contained in this article reflect only the authors' views  
724 and not that of the EU, the European Union Horizon 2020 or any other body.  
725

## 726 Software

727 All images were processed in Google Earth Engine.  
728

## 729 CRediT authorship contribution statement

730 **Felicia O. Akinyemi**: Conceptualization, Survey design and reference data collection,  
731 Methodology, Formal analysis, Visualization, Writing – original draft, Writing – review &  
732 editing, Funding acquisition. **Philippe Rufin**: Conceptualization, Methodology, Formal  
733 analysis, Software, Visualization, Writing – original draft, Writing – review & editing. **Esther**  
734 **Shupel Ibrahim**: Methodology, Writing – review & editing. **Patrick Hostert**: Methodology,  
735 Writing – review & editing. **Lucia O. Ogunsumi**: Cropping calendar and survey design,  
736 Agricultural Development Programme and Extension services. **Olugbenga A. Egbetokun**:  
737 Cropping calendar, Farmers' Survey. **Chinwe Ifejika Speranza**: Conceptualization, Writing  
738 – review & editing, Supervision, Funding acquisition.

## 739 Declaration of Competing Interest

740  
741 The authors declare that they have no known competing financial interests or personal  
742 relationships, and neither has any funder influenced the work reported in this paper at any stage  
743 from design to submission.  
744

745 **Data availability**

746

747 Sources of all datasets used are specified in the manuscript. Data are made available in Zenodo  
748 after acceptance.

749

750 **References**

751 Abubakar, G.A., Wang, K., Koko, A.F., Husseini, M.I., Shuka, K.A.M., Deng, J., Gan, M.  
752 (2023). Mapping maize cropland and land cover in semi-arid region in northern  
753 Nigeria using Machine Learning and Google Earth Engine. *Remote Sensing*  
754 15(11):2835. <https://doi.org/10.3390/rs15112835>

755 Akinyemi, F.O. (2013). An assessment of land use change in the cocoa belt of south west  
756 Nigeria. *International Journal of Remote Sensing*, 34(8): 2858-2875.  
757 <https://doi.org/10.1080/01431161.2012.753167>

758 Akinyemi, F.O. (2017). Climate change and variability in semi-arid Palapye, Eastern  
759 Botswana: An assessment from smallholder farmers' perspective. *Weather Clim. Soc.*,  
760 9:349-65. <https://doi.org/10.1175/WCAS-D-16-0040.1>

761 Akinyemi, F.O., Ifejika Speranza, C. (2022). Agricultural landscape change impact on the  
762 quality of land: An African continent-wide assessment in gained and displaced  
763 agricultural lands. *International Journal of Applied Earth Observations and*  
764 *Geoinformation*, 106:102644. <https://doi.org/10.1016/j.jag.2021.102644>

765 Ayoola, O.T., Makinde, E.A. (2007). Fertilizer treatment effects on performance of cassava  
766 under two planting patterns in a cassava-based cropping system in South West Nigeria.  
767 *Res. J. Agric. Biol. Sci.*, 3 (1), 13–20.

768 Becker-Reshef, I., Barker, B., Whitcraft, A., Oliva, P., Mobley, K., Justice C., Sahajpal, R.  
769 (2023). Crop type maps for operational global agricultural monitoring. *Scientific Data*,  
770 10, 172. <https://doi.org/10.1038/s41597-023-02047-9>

771 Bizikova, L., De Brauw, A., Rose, M.E., Laborde, D., Motsumi, K., Murphy, M., Parent,  
772 M., Picard, F., Smaller, C. (2022). Achieving sustainable food systems in a global  
773 crisis: Nigeria country roadmap to end hunger, double farmer incomes, improve diets,  
774 and protect the climate. International Institute for Sustainable Development.  
775 [https://www.iisd.org/system/files/2022-09/sustainable-food-systems-global-crisis-](https://www.iisd.org/system/files/2022-09/sustainable-food-systems-global-crisis-nigeria.pdf)  
776 [nigeria.pdf](https://www.iisd.org/system/files/2022-09/sustainable-food-systems-global-crisis-nigeria.pdf) [accessed 15 Nov. 2023].

777 Bouws, H., Finckh, M.R. (2008). Effects of strip intercropping of potatoes with non-hosts  
778 on late blight severity and tuber yield in organic production. *Plant Path* 57, 916–927.

779 Breiman, L. (2001). Random forests. *Machine Learning*, 45:5-32.  
780 <https://doi.org/10.1023/A:1010933404324>

781 Banerjee, R., Carletto, C., Jolliffe, D.M. (2015). From tragedy to renaissance: Improving  
782 agricultural data for better policies. Policy research working paper no. WPS 7150,  
783 LSMS, Washington, D.C.: World  
784 Bank. <http://documents.worldbank.org/curated/en/313131468194048389/From->



- 785 [tragedy-to-renaissance-improving-agricultural-data-for-better-policies](#) [Accessed 15  
786 Nov. 2023]
- 787 Chiaka, J.C., Zhen, L., Yunfeng, H., Xiao, Y., Muhirwa, F., Lang, T. (2022). Smallholder  
788 farmers contribution to food production in Nigeria. *Front. Nutr.* 9:916678.  
789 <https://doi.org/10.3389/fnut.2022.916678>
- 790 Danso, D.K., Anquetin, S., Diedhiou, A., Lavaysse, C., Koba, A., Touré, N.D.E. (2019).  
791 Spatio-temporal variability of cloud cover types in West Africa with satellite-based  
792 and reanalysis data. *Quarterly Journal of the Royal Meteorological Society*, 145(725):  
793 3715-3731.
- 794 Ekong, E.E. (1983). Farm size, agricultural and rural development in Nigeria. *Agricultural*  
795 *Administration*, 14(3): 169-183. [https://doi.org/10.1016/0309-586X\(83\)90014-6](https://doi.org/10.1016/0309-586X(83)90014-6)
- 796 Famine Early Warning System Network (2023a). Nigeria Food Security Outlook, June  
797 2023 - January 2024. FEWS NET. [https://reliefweb.int/report/nigeria/nigeria-food-](https://reliefweb.int/report/nigeria/nigeria-food-security-outlook-june-2023-january-2024)  
798 [security-outlook-june-2023-january-2024](https://reliefweb.int/report/nigeria/nigeria-food-security-outlook-june-2023-january-2024) [Accessed 01 Dec. 2023].
- 799 Famine Early Warning System Network (2023b). Nigeria Food Security Outlook,  
800 October 2023 - May 2024. FEWS NET. [https://reliefweb.int/report/nigeria/nigeria-](https://reliefweb.int/report/nigeria/nigeria-food-security-outlook-october-2023-may-2024)  
801 [food-security-outlook-october-2023-may-2024](https://reliefweb.int/report/nigeria/nigeria-food-security-outlook-october-2023-may-2024) [Accessed 01 Dec. 2023].
- 802 FAO (2014). The state of food and agriculture 2014: Innovation in family farming food  
803 and agriculture organization of the United Nations.  
804 [https://policycommons.net/artifacts/2071892/the-state-of-food-and-agriculture-sofa-](https://policycommons.net/artifacts/2071892/the-state-of-food-and-agriculture-sofa-2014/2827191/)  
805 [2014/2827191/](https://policycommons.net/artifacts/2071892/the-state-of-food-and-agriculture-sofa-2014/2827191/) [Accessed 01 Dec. 2023].
- 806 FAO (2016). The state of food and agriculture: Climate change, agriculture and food  
807 security. FAO, Rome. <https://www.fao.org/3/i6030e/I6030E.pdf> [Accessed 01 Dec.  
808 2023].
- 809 Fatunbi, A.O., Ajayi, M.T., Akinbamijo, O.O. (2020). Strategies for transforming  
810 smallholder farming in Africa. *Forum for Agricultural Research in Africa (FARA)*,  
811 Accra Ghana, pp. 1-121 Available online at [https://library.faraafrica.org/mp-](https://library.faraafrica.org/mp-files/strategies-for-transforming-smallholder-farming-in-africa-ofatunbi.pdf)  
812 [files/strategies-for-transforming-smallholder-farming-in-africa-ofatunbi.pdf](https://library.faraafrica.org/mp-files/strategies-for-transforming-smallholder-farming-in-africa-ofatunbi.pdf)  
813 [accessed 2023 May 27]
- 814 Fritz, S., See, L., Bayas, J.C.L., Waldner, F., Jacques, D., Becker-Reshef, I., Whitcraft, A.,  
815 Baruth, B., Bonifacio, R., Crutchfield, J., Rembold, F., Rojas, O., Schucknecht, A.,  
816 Van der Velde, M., Verdin, J., Wu, B., Yan, N., You, L., Gilliams, S., Mücher, S.,  
817 Tetrault, R., Moorthy, I., McCallum, I. (2019). A comparison of global agricultural  
818 monitoring systems and current gaps. *Agricultural Systems*, 168, 258-272.  
819 <https://doi.org/10.1016/j.agsy.2018.05.010>.
- 820 Gorelick, N., Hancher, M., Dixon, M., Ilyushchenko, S., Thau, D., & Moore, R. (2017).  
821 Google Earth Engine: Planetary-scale geospatial analysis for everyone. *Remote*  
822 *Sensing of Environment*, 202:18-27. <https://doi.org/10.1016/j.rse.2017.06.031>
- 823 Griffiths, P., Nendel, C., Hostert, P. (2019). Intra-annual reflectance composites from  
824 Sentinel-2 and Landsat for national-scale crop and land cover mapping. *Remote Sens.*  
825 *Environ.*, 220, 135–151.

- 826 Ibrahim, E.S., Rufin, R., Nill, L., Kamali, B., Nendel, C., Hostert, P. (2021). Mapping crop  
827 types and cropping systems in Nigeria with Sentinel-2 imagery. *Remote Sensing*  
828 13(17), 3523. <https://doi.org/10.3390/rs13173523>
- 829 Iloeje, N.P. (2001). *A new geography of Nigeria (new revised edition)*. Longman Nig. Ltd:  
830 Lagos, Nigeria, p.200.
- 831 Jayne, T.S., Wineman, A., Chamberlin, J., Muyanga, M., Yeboah, F.K. (2022). Changing  
832 farm size distributions and agricultural transformation in Sub-Saharan Africa. *Annu.*  
833 *Rev. Resour. Econ.* 14, 109–130. [https://doi.org/10.1146/annurev-resource-111220-](https://doi.org/10.1146/annurev-resource-111220-025657)  
834 [025657](https://doi.org/10.1146/annurev-resource-111220-025657)
- 835 Jin, Z., Azzari, G., You, C., Di Tommaso, S., Aston, S., Burke, M., Lobell, D.B. (2019).  
836 Smallholder maize area and yield mapping at national scales with Google Earth  
837 Engine. *Remote Sensing of Environment* 228, 115-128.  
838 <https://doi.org/10.1016/j.rse.2019.04.016>
- 839 Johnson, D.J. (2014). An assessment of pre- and within-season remotely sensed variables  
840 for forecasting corn and soybean yields in the United States. *Remote Sensing of*  
841 *Environment*, 141, 116-128. <https://doi.org/10.1016/j.rse.2013.10.027>
- 842 Karlson, M., Ostwald, M., Bayala, J., Bazié, H.R., Ouedraogo, A.S., Soro, B., Sanou, J.,  
843 Reese, H. (2020). The potential of Sentinel-2 for crop production estimation in a  
844 smallholder agroforestry landscape, Burkina Faso. *Front. Environ. Sci.* 8.  
845 <https://doi.org/10.3389/fenvs.2020.00085>
- 846 Khabbazan, S., Vermunt, P., Steele-Dunne, S., Ratering Arntz, L., Marinetti, C., van der  
847 Valk, D., Iannini, L., Molijn, R., Westerdijk, K., van der Sande, C. (2019). Crop  
848 monitoring using Sentinel-1 data: A case study from The Netherlands. *Remote*  
849 *Sensing*, 11(16): 1887. <https://doi.org/10.3390/rs11161887>
- 850 Kingma, D.P., Ba, J. (2017). Adam: A method for stochastic optimization. 3<sup>rd</sup> International  
851 Conference for Learning Representations, San Diego.  
852 <https://doi.org/10.48550/arXiv.1412.6980>
- 853 Kinyua, M.W., Kihara, J., Bekunda, M., Bolo, P., Mairura, F.S., Fischer, G., Mucheru-  
854 Muna, M.W. (2023). Agronomic and economic performance of legume-legume and  
855 cereal-legume intercropping systems in Northern Tanzania. *Agricultural Systems* 205,  
856 103589. <https://doi.org/10.1016/j.agsy.2022.103589>.
- 857 Kolawole, P.O., Agbetoye, L., Ogunlowo, S.A. (2010). Sustaining world food security with  
858 improved cassava processing technology: The Nigeria experience. *Sustainability* 2,  
859 3681–3694.
- 860 Kpienbaareh, D., Sunm X., Wang, J., Luginaah, I., Bezner, K.R., Lupafya, E., Dakishoni,  
861 L. (2021). Crop type and land cover mapping in northern Malawi using the integration  
862 of Sentinel-1, Sentinel-2, and PlanetScope satellite data. *Remote Sensing*, 13(4):700.  
863 <https://doi.org/10.3390/rs13040700>
- 864 Lambert, M.-J., Traoré, P.C.S., Blaes, X., Baret, P., Defourny, P. (2018). Estimating  
865 smallholder crops production at village level from Sentinel-2 time series in Mali's

- 866 cotton belt. *Remote Sensing of Environment*, 216, 647–657.  
867 <https://doi.org/10.1016/j.rse.2018.06.036>
- 868 Lesiv, M., Laso Bayas, J.C., See, L., Duerauer, M., Dahlia, D., Durando, N., Hazarika, R.,  
869 Kumar Sahariah, P., Vakolyuk, M., Blyshchyk, V. (2019). Estimating the global  
870 distribution of field size using crowdsourcing. *Glob. Chang. Biol.* 25 (1), 174-186.  
871 <https://doi.org/10.1111/gcb.14492>
- 872 Lowder, S.K., Sánchez, M.V., Bertini, R. (2021). Which farms feed the world and has  
873 farmland become more concentrated? *World Development*, 142, 105455.  
874 <https://doi.org/10.1016/j.worlddev.2021.105455>
- 875 Mazarire, T.T., Ratshiedana, P.E., Nyamugama, A., Adam, E., Chirima, G. (2020).  
876 Exploring machine learning algorithms for mapping crop types in a heterogeneous  
877 agriculture landscape using Sentinel-2 data. A case study of Free State Province, South  
878 Africa. *South African Journal of Geomatics* 9(2):333-347.  
879 <https://doi.org/10.4314/sajg.v9i2.22>
- 880 Menashe, D., Friedl, M.A. (2018). User Guide to Collection 6 MODIS Land Cover  
881 (MCD12Q1 and MCD12C1) Product Sull-  
882 [https://lpdaac.usgs.gov/documents/101/MCD12\\_User\\_Guide\\_V6.pdf](https://lpdaac.usgs.gov/documents/101/MCD12_User_Guide_V6.pdf) [Accessed 01  
883 Dec. 2023]
- 884 Ministry of Agriculture and Natural Resources (1959). Future Policy of the Ministry of  
885 Agriculture and Natural Resources. Ibadan: Government Printer, p. 12.
- 886 Muyanga, M., Aromolaran, A., Jayne, T., Liverpool-Tasie, S., Awokuse, T., Adelaja, A.  
887 (2019). Changing farm structure and agricultural commercialisation in Nigeria.  
888 Agricultural Policy Research Policy in Africa working paper 26, Future Agricultures  
889 Consortium. <https://opendocs.ids.ac.uk/opendocs/handle/20.500.12413/16699>
- 890 Nwokoro, C.C., Kreye, C., Necpalova, M., Adeyemi, O., Busari, M., Tariku, M., Tokula,  
891 M., Olowokere, F., Pypers, P., Hauser, S., Six, J. (2021). Developing recommendations  
892 for increased productivity in cassava-maize intercropping systems in Southern Nigeria.  
893 *Field Crops Research* 272,108283. <https://doi.org/10.1016/j.fcr.2021.108283>
- 894 Olasantan, F.O., Ezumah, H.C., Lucas, E.O. (1996). Effects of intercropping with maize  
895 on the micro-environment, growth and yield of cassava. *Agric. Ecosyst. Environ.* 57  
896 (2),149–158. [https://doi.org/10.1016/0167-8809\(96\)01019-5](https://doi.org/10.1016/0167-8809(96)01019-5)
- 897 Olofsson, P., Foody, G.M., Herold, M., Stehman, S.V., Woodcock, C.E., Wulder, M.A.  
898 (2014). Good practices for estimating area and assessing accuracy of land change.  
899 *Remote Sensing of Environment* 148, 42-57.  
900 <https://doi.org/10.1016/j.rse.2014.02.015>.
- 901 Omotilewa, O.J., Jayne, T.S., Muyanga, M., Aromolaran, A.B., Liverpool-Tasie, L.S.O.,  
902 Awokuse, T. (2021). A revisit of farm size and productivity: Empirical evidence from  
903 a wide range of farm sizes in Nigeria. *World Development* 146, 105592.  
904 <https://doi.org/10.1016/j.worlddev.2021.105592>
- 905 Ouzemou, J.-E., El Harti, A., Lhissou, R., El Moujahid, A., Bouch, N., El Ouazzani, R.,  
906 Bachaoui, E.M., El Ghmari, A. (2018). Crop type mapping from pansharpened Landsat

- 907 8 NDVI data: A case of a highly fragmented and intensive agricultural system. *Remote*  
908 *Sensing Applications: Society and Environment*, 11, 94-103.
- 909 Planque, C., Lucas, R., Punalekar, S., Chognard, S., Hurford, C., Owers, C., Horton, C.,  
910 Guest, P., King, S., Williams, S., et al. (2021). National crop mapping using Sentinel-  
911 1 time series: A knowledge-based descriptive algorithm. *Remote Sens.*, 13, 846.  
912 <https://doi.org/10.3390/rs13050846>
- 913 Rao, P., Zhou, W., Bhattarai, N., Srivastava, A.K., Singh, B., Poonia, S., Lobell, D.B., Jain,  
914 M. (2021). Using Sentinel-1, Sentinel-2, and Planet imagery to map crop type of  
915 smallholder farms. *Remote Sensing*, 13(10),1870. <https://doi.org/10.3390/rs13101870>
- 916 Ren, T., Xu, H., Cai, X., Yu, S., Qi, J. (2022). Smallholder crop type mapping and rotation  
917 monitoring in mountainous areas with Sentinel-1/2 imagery. *Remote Sensing*, 14(3),  
918 566. <https://doi.org/10.3390/rs14030566>
- 919 Samberg, L.H., Gerber, J.S., Ramankutty, N., Herrero, M., West, P.C. (2016). Subnational  
920 distribution of average farm size and smallholder contributions to global food  
921 production. *Environ. Res. Lett.* 11(12), 124010. <https://doi.org/10.1088/1748-9326/>
- 922 Ricciardi, V., Ramankutty, N., Mehrabi, Z., Jarvis, L., Chookolingo, B. (2018). How much  
923 of the world's food do smallholders produce? *Global Food Security*, 17, 64-72.  
924 <https://doi.org/10.1016/j.gfs.2018.05.002>
- 925 Rufin, P., Bey, A., Picoli, M., Meyfroidt, P. (2022). Large-area mapping of active cropland  
926 and short-term fallows in smallholder landscapes using PlanetScope data. *International*  
927 *Journal of Applied Earth Observation and Geoinformation*, 112, 102937.  
928 <https://doi.org/10.1016/j.jag.2022.102937>
- 929 Sothe, C., Almeida, C.M., Liesenberg, V., Schimalski, M.B. (2017). Evaluating sentinel-2  
930 and Landsat-8 data to map successional forest stages in a subtropical forest in Southern  
931 Brazil. *Remote Sensing* 9, 838.
- 932 Stumpf, A., Lachiche, N., Malet, J.-P., Kerle, N., Puissant, A. (2014). Active learning in  
933 the spatial domain for Remote Sensing image classification. *IEEE Trans. Geosci.*  
934 *Remote Sensing*, 52(5):2492–2507. <https://doi.org/10.1109/TGRS.2013.2262052>
- 935 Srivastava, A.M., Ewert, F., Akinwumiju, A.S., Zeng, W., Ceglar, A., Ezui, K.S.,  
936 Adelodun, A., Adebayo, A., Sobamowo, J., Singh, M., Rahimi, J., Gaiser, T. (2023).  
937 Cassava yield gap—A model-based assessment in Nigeria. *Front. Sustain. Food Syst.*  
938 *Sec. Agroecology and Ecosystem Services*, 6.  
939 <https://doi.org/10.3389/fsufs.2022.1058775>
- 940 Taiwo, B.E., Al Kafy, A., Samuel, A.A., Rahaman, Z.A., Ayowole, O.E., Shahrier, M.,  
941 Duti, B.M., Rahman, M.T., Peter, O.T., Abosede, O.O. (2023). Monitoring and  
942 predicting the influences of land use/land cover change on cropland characteristics and  
943 drought severity using remote sensing techniques. *Environmental and Sustainability*  
944 *Indicators*, 18, 100248. <https://doi.org/10.1016/j.indic.2023.100248>.
- 945 Tuia, D., Pasolli, E., Emery, W.J. (2011). Using active learning to adapt remote sensing  
946 image classifiers. *Remote Sensing of Environment*, 115(9):2232–2242.  
947 <https://doi.org/10.1016/j.rse.2011.04.022>

- 948 Veloso, A., Mermoz, S., Bouvet, A., Le Toan, T., Planells, M., Dejoux, J.F., Ceschia, E.  
949 (2017). Understanding the temporal behavior of crops using Sentinel-1 and Sentinel-  
950 2-like data for agricultural applications. *Remote Sensing of Environment*, 199, 415–  
951 426.
- 952 Vreugdenhil, M., Wagner, W., Bauer-Marschallinger, B., Pfeil, I., Teubner, I., Rüdiger, C.,  
953 Strauss, P. (2018). Sensitivity of Sentinel-1 backscatter to vegetation dynamics: An  
954 Austrian case study. *Remote Sens.*, 10, 1396.
- 955 Waldner, F., Diakogiannis, F.I. (2020). Deep learning on edge: Extracting field boundaries  
956 from satellite images with a convolutional neural network. *Remote Sens. Environ.*,  
957 245, 111741.
- 958 Wang, S., Waldner, F., Lobell, D.B. (2022). Unlocking large-scale crop field delineation  
959 in smallholder farming systems with Transfer Learning and Weak Supervision.  
960 *Remote Sensing*, 14(22):5738. <https://doi.org/10.3390/rs14225738>
- 961 Whitcraft, A.K., Vermote, E.F., Becker-Reshef, I., Justice, C.O. (2015). Cloud cover  
962 throughout the agricultural growing season: Impacts on passive optical earth  
963 observations. *Remote Sens. Environ.*, 156, 438–447.

964

#### 965 **Web references**

- 966 FAO (2015). A data portrait of smallholder farmers.  
967 [https://www.fao.org/fileadmin/templates/esa/smallholders/Concept\\_Smallholder\\_Dat](https://www.fao.org/fileadmin/templates/esa/smallholders/Concept_Smallholder_Dataportrait_web.pdf)  
968 [aportrait\\_web.pdf](https://www.fao.org/fileadmin/templates/esa/smallholders/Concept_Smallholder_Dataportrait_web.pdf) [Accessed 02 Sept. 2023]
- 969 United Nations (2015). *Transforming our World: The 2030 Agenda for Sustainable*  
970 *Development*. A/RES/70/1. [21252030 Agenda for Sustainable Development web.pdf](https://www.un.org/sustainabledevelopment/)  
971 [\(un.org\)](https://www.un.org/sustainabledevelopment/) [Accessed 04 Jan. 2023].
- 972 United Nations (2017). United Nations Decade of Family Farming (2019-2028). 72<sup>nd</sup> UN  
973 General Assembly. A/c.2/72/L.12/Rev1. <https://digitallibrary.un.org/record/1479766>  
974 [Accessed 01 Dec. 2023].

#### 975 **Data references**

- 976 ESA 2021. Product Validation Report (D12-PVR), WorldCover\_PVR\_v2.  
977 [https://worldcover2021.esa.int/data/docs/WorldCover\\_PVR\\_V2.0.pdf](https://worldcover2021.esa.int/data/docs/WorldCover_PVR_V2.0.pdf) [Accessed 01  
978 Dec. 2023].
- 979 ESRI 2021. Living atlas <https://livingatlas.arcgis.com/landcover/> [Accessed 01 Dec. 2023].
- 980 Planet Team (2022). Planet Application Program Interface: In space for life on Earth. San  
981 Francisco, CA. <https://api.planet.com> [Accessed 06 Jan. 2023].
- 982 Planet-NICFI (2023). Norway's International Climate and Forest Initiative Satellite  
983 program collection. <https://www.planet.com/nicfi/> [Accessed 06 Jan. 2023].